Wheat zinc finger protein TaZF interacts with both the powdery mildew AvrPm2 protein and the corresponding wheat Pm2a immune receptor

Manser, Beatrice ; Zbinden, Helen ; Herren, Gerhard ; Steger, Joel ; Isaksson, Jonatan ; Bräunlich, Stephanie ; Wicker, Thomas ; Keller, Beat

Abstract: Plant defense responses to pathogens are induced after direct or indirect perception of effector proteins or their activity on host proteins. In fungal-plant interactions, relatively little is known about whether, in addition to avirulence effectors and immune receptors, other proteins contribute to specific recognition. The nucleotide-binding leucine-rich repeat (NLR) immune receptor Pm2a in wheat recognizes the fungal powdery mildew effector AvrPm2. We found that the predicted wheat zinc finger TaZF interacts with both the fungal avirulence protein AvrPm2 and the wheat NLR Pm2a. We further demonstrated that the virulent AvrPm2-H2 variant does not interact with TaZF. TaZF silencing in wheat resulted in a reduction but not a loss of Pm2a-mediated powdery mildew resistance. Interaction studies showed that the leucine-rich repeat domain of Pm2a is the mediator of the interaction with TaZF. TaZF recruits both Pm2a and AvrPm2 from the cytosol to the nucleus, resulting in nuclear localization of Pm2a, TaZF, and AvrPm2 in wheat. We propose that TaZF acts as a facilitator of Pm2a-dependent AvrPm2 effector recognition. Our findings highlight the importance of identifying effector host targets for characterization of NLR-mediated effector recognition.

DOI: https://doi.org/10.1016/j.xplc.2023.100769

Plant Communications
Research article

CellPress
Partner Journal

Wheat zinc finger protein TaZF interacts with both the powdery mildew AvrPm2 protein and the corresponding wheat Pm2a immune receptor

Beatrice Manser[1,3], Helen Zbinden[1], Gerhard Herren[1], Joel Steger[1], Jonatan Isaksson[1], Stephanie Bräunlich[1,2], Thomas Wicker[1] and Beat Keller[1,*]

[1]Department of Plant and Microbial Biology, University of Zurich, Zollikerstrasse 107, 8008 Zurich, Switzerland

[2]Present address: Agroscope, Route de Duillier 50, 1260 Nyon, Switzerland

[3]Present address: BIOREBA AG, Christoph Merian-Ring 7, 4153 Reinach, Switzerland

***Correspondence: Beat Keller (bkeller@botinst.uzh.ch)**

https://doi.org/10.1016/j.xplc.2023.100769

ABSTRACT

Plant defense responses to pathogens are induced after direct or indirect perception of effector proteins or their activity on host proteins. In fungal–plant interactions, relatively little is known about whether, in addition to avirulence effectors and immune receptors, other proteins contribute to specific recognition. The nucleotide-binding leucine-rich repeat (NLR) immune receptor Pm2a in wheat recognizes the fungal powdery mildew effector AvrPm2. We found that the predicted wheat zinc finger TaZF interacts with both the fungal avirulence protein AvrPm2 and the wheat NLR Pm2a. We further demonstrated that the virulent AvrPm2-H2 variant does not interact with TaZF. *TaZF* silencing in wheat resulted in a reduction but not a loss of Pm2a-mediated powdery mildew resistance. Interaction studies showed that the leucine-rich repeat domain of Pm2a is the mediator of the interaction with TaZF. TaZF recruits both Pm2a and AvrPm2 from the cytosol to the nucleus, resulting in nuclear localization of Pm2a, TaZF, and AvrPm2 in wheat. We propose that TaZF acts as a facilitator of Pm2a-dependent AvrPm2 effector recognition. Our findings highlight the importance of identifying effector host targets for characterization of NLR-mediated effector recognition.

Key words: plant immunity, plant–fungal interactions, pathogen effectors, nucleotide-binding leucine-rich repeat, immune receptor, NLR, wheat, powdery mildew

Manser B., Zbinden H., Herren G., Steger J., Isaksson J., Bräunlich S., Wicker T., and Keller B. (2023). Wheat zinc finger protein TaZF interacts with both the powdery mildew AvrPm2 protein and the corresponding wheat Pm2a immune receptor. Plant Comm. **4**, 100769.

INTRODUCTION

The plant immune system is essentially composed of two types of immune receptors. The cell-surface-localized pattern recognition receptors can detect conserved pathogen-associated molecular patterns (PAMPs) such as the fungal cell-wall component chitin and induce PAMP-triggered immunity (PTI) (Boutrot and Zipfel, 2017; Zhou and Zhang, 2020). Fungal and oomycete pathogens secrete hundreds of effector proteins via the haustorium into the plant cell, where they interact with various host proteins to interfere with plant defense responses and facilitate pathogen infection (Petre and Kamoun, 2014; Lo Presti et al., 2015; Toruño et al., 2016). In return, plants have evolved a second type of immune receptor, the intracellular nucleotide-binding leucine-rich repeat receptors (NLRs), which can specifically recognize pathogen-derived effectors either directly or indirectly (Duxbury et al., 2016; Chen et al., 2022). Some NLRs can indirectly recognize the presence of a specific effector by monitoring an effector target and detecting the modification of the target by an effector (Cesari, 2017; Nguyen et al., 2021; Saur et al., 2021). Direct effector recognition is the dominant form of resistance to filamentous pathogens such as fungi and oomycetes, whereas indirect effector recognition has been more often described for bacteria (Figueroa et al., 2021; Chen et al., 2022). One of the first-characterized direct NLR–Avr interactions was between the flax NLR protein L and the effector AvrL567 from the flax rust fungus *Melampsora lini* (Dodds et al., 2006). Recognition of an effector by the corresponding NLR leads to effector-triggered immunity (ETI), typically resulting in a

Published by the Plant Communications Shanghai Editorial Office in association with Cell Press, an imprint of Elsevier Inc., on behalf of CSPB and CEMPS, CAS.

Please cite this article in press as: Manser et al., Wheat zinc finger protein TaZF interacts with both the powdery mildew AvrPm2 protein and the corresponding wheat Pm2a immune receptor, Plant Communications (2023), https://doi.org/10.1016/j.xplc.2023.100769

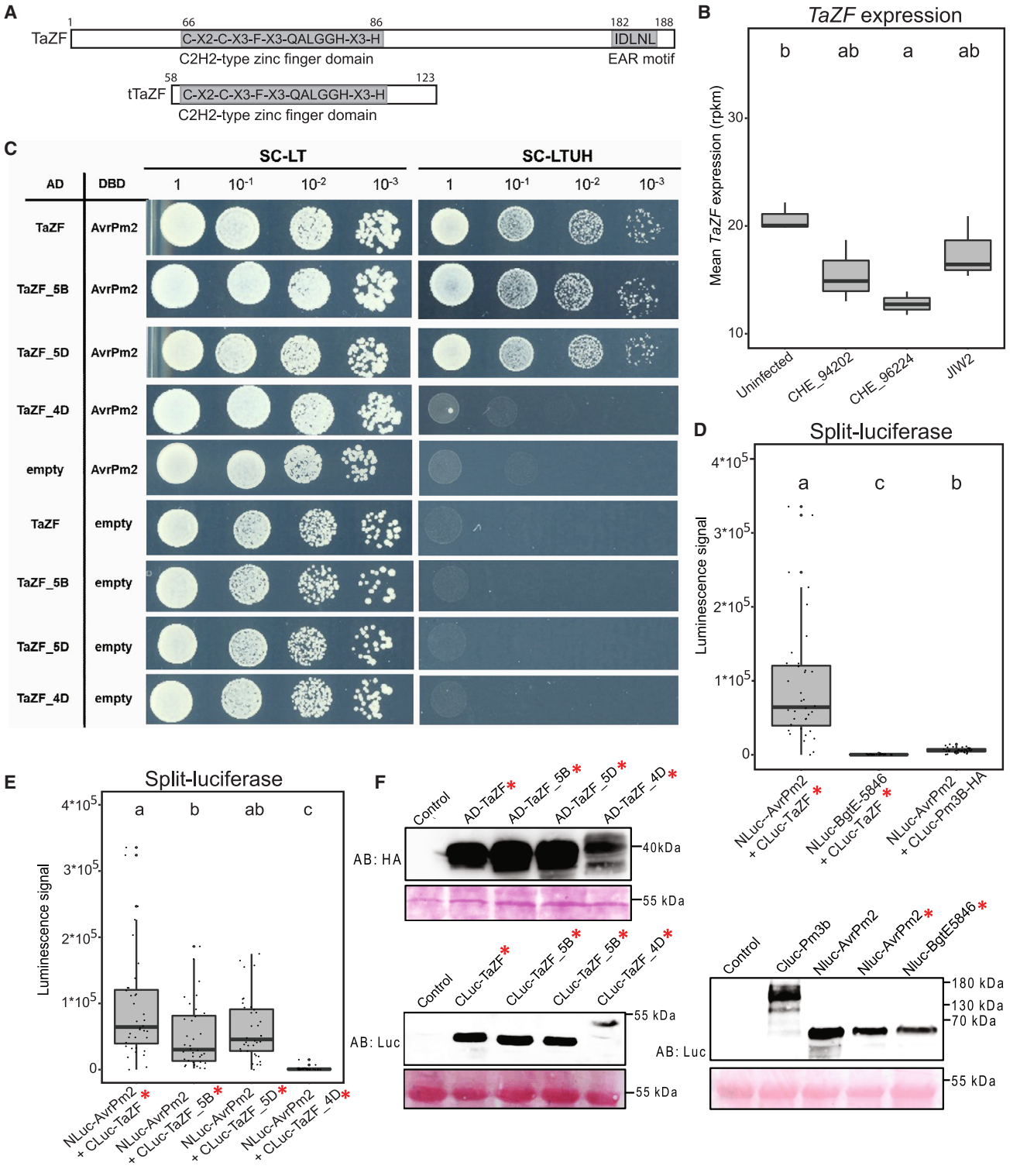

Figure 1. AvrPm2 interacts with the predicted wheat transcription factor TaZF.

(A) Schematic representation of TaZF and the truncated TaZF mutant tTaZF. Conserved motifs, domains, and amino acid positions are indicated.

(B) Expression levels of *TaZF* in the susceptible wheat cultivar Chinese Spring infected with the *Bgt* isolate CHE_94202, CHE_96224, or JIW2. Expression of *TaZF* is displayed as reads per kilobase pair per million reads (rpkm), which were obtained from three independent experiments.

(C) Yeast two-hybrid assay reveals interaction of AvrPm2 with full-length TaZF and TaZF homeologs. Growth of transformants was determined on SC-LT medium, and protein interactions were determined by growth of yeast on SC-LTUH. Photographs were taken after 4 days of incubation and are representative of at least three independent experiments using yeast obtained from three independent yeast transformations.

(legend continued on next page)

Please cite this article in press as: Manser et al., Wheat zinc finger protein TaZF interacts with both the powdery mildew AvrPm2 protein and the corresponding wheat Pm2a immune receptor, Plant Communications (2023), https://doi.org/10.1016/j.xplc.2023.100769

localized hypersensitive cell-death response (HR), but also in non-lethal defense responses such as papillae formation and cell-wall fortification in the case of powdery mildew resistance (Troch et al., 2014; Chen et al., 2022). Common transcription and signal transduction pathways triggered by PTI and ETI (Ngou et al., 2021; Yuan et al., 2021) are often the point of action for effectors. Over 50% of the identified host proteins targeted by fungal effectors are involved in transcription and signaling (He et al., 2020). Enzymatic activity has not been described for most fungal effectors, including those that act as avirulence factors. Instead, their mode of action may be to disrupt the formation of biologically active protein complexes in order to modify host transcriptional processes (He et al., 2020; Saur et al., 2021).

Blumeria graminis is an ascomycete fungal pathogen with an obligately biotrophic lifestyle that causes the disease powdery mildew on cereals. Powdery mildew specifically growing on wheat (*B. graminis* f. sp. *tritici*, *Bgt*) and powdery mildew growing on barley (*B. graminis* f. sp. *hordei*, *Bgh*) are agronomically important pathogens (Dean et al., 2012). The genomes of *Bgt* and *Bgh* encode over 800 candidate effector proteins (Frantzeskakis et al., 2018; Müller et al., 2019). The effectors recognized by plant NLRs represent avirulence (Avr) proteins and are of great interest because their presence has a decisive effect on the host–powdery mildew interaction. The *Bgh* effectors Avr_{a1}, Avr_{a6}, Avr_{a7}, Avr_{a9}, Avr_{a10}, Avr_{a13}, and Avr_{a22} are specifically recognized by different allelic variants of the barley NLR Mla, whereas Avr_{k1} is recognized by the barley NLR Mlk1 (Ridout et al., 2006; Lu et al., 2016; Saur et al., 2019; Bauer et al., 2021). In *Bgt*, AvrPm2 is recognized by the wheat NLR Pm2a, whereas the *Bgt* effectors $AvrPm3^{a2/f2}$, $AvrPm3^{b2/c2}$, and $AvrPm3^{d3}$ are recognized by different variants of the wheat Pm3 resistance protein encoded by the *Pm3* allelic series (Bourras et al., 2015, 2019; Praz et al., 2017). Co-expression of the *Bgh* effectors Avr_{a1}, Avr_{a6}, Avr_{a7}, Avr_{a10}, Avr_{a13}, and Avr_{a22} and the *Bgt* effectors *AvrPm1a*, *AvrPm2*, $AvrPm3^{a2/f2}$, $AvrPm3^{b2/c2}$, $AvrPm3^{d3}$, *AvrPm8*, and *AvrPm17* with their corresponding NLRs caused HR in *Nicotiana benthamiana* (Bourras et al., 2015, 2019; Praz et al., 2017; Saur et al., 2019; Bauer et al., 2021; Hewitt et al., 2021; Müller et al., 2022; Kunz et al., 2023). This suggests that either the NLRs recognize the effectors directly or that the additional proteins needed for HR induction after NLR–Avr recognition are conserved among wheat and *N. benthamiana*. Indeed, direct interactions of the barley Mla variants Mla7, Mla10, and Mla13 with their corresponding avirulence effectors were found in luciferase complementation and yeast two-hybrid (Y2H) assays (Saur et al., 2019). The *Bgt* effector AvrPm2 belongs to the AvrPm2 effector family, all members of which have a predicted RNase-like structure with homology to the ribonuclease T1 from *Aspergillus phoenicis* (RNase-like) (Praz et al., 2017). The RNase-like structure was confirmed by X-ray crystallography of the *Bgh* effector and the AvrPm2 family member CSEP0064/BEC1054 (Pennington et al., 2019), as well as AvrPm2 (Cao et al., 2023). The NLR Pm2a was isolated from hexaploid wheat and recognizes AvrPm2 (Sánchez-Martín et al., 2016; Praz et al., 2017). In a previous study, seven additional *Pm2* alleles, as well as the virulent *AvrPm2-H2* haplotype, were identified (Manser et al., 2021). The molecular interactions between AvrPm2 and Pm2 remain elusive.

In this study, we found that the predicted wheat zinc finger protein TaZF interacts with both the powdery mildew effector protein AvrPm2 and the corresponding wheat NLR immune receptor Pm2a. We demonstrated that the interaction of Pm2a with TaZF is independent of AvrPm2 in a split-luciferase assay; that the leucine-rich repeat (LRR) domain of Pm2a interacts with AvrPm2a in a co-immunoprecipitation (coIP) assay; and that addition of AvrPm2 leads to detectable interaction of full-length Pm2a, TaZF, and AvrPm2 in a coIP assay. We found that the three proteins co-localize in the nucleus, both in *N. benthamiana* and in wheat. We also found that silencing of *TaZF* in wheat led to decreased Pm2a-mediated powdery mildew resistance. Using a truncated Pm2a protein, we showed that the LRR domain of Pm2a mediates its direct interaction with TaZF. Our study of Pm2a-mediated AvrPm2 recognition reveals an interaction of a putative wheat transcription factor with an avirulence protein as well as its corresponding NLR immune receptor.

RESULTS

AvrPm2 interacts with the predicted wheat zinc finger protein TaZF

Given the frequent observation of direct interactions between NLRs and fungal Avrs, we first assessed whether there was a physical interaction between Pm2a and AvrPm2 by performing Y2H experiments and split-luciferase assays (Gehl et al., 2011). Although we used experimental approaches that have been used to demonstrate the direct interaction between MLA and Avra proteins (Saur et al., 2019), we did not find any evidence for a direct interaction between full-length Pm2a and AvrPm2 (Supplemental Figure 1 and Supplemental Note 1). These results indicated that additional wheat proteins might contribute to Pm2a-mediated AvrPm2 recognition. To identify candidate wheat proteins that interact with AvrPm2 and might be involved in Pm2a-mediated AvrPm2 recognition, we performed a Y2H screen in which we tested AvrPm2 as an effector bait against a cDNA prey library prepared from hexaploid wheat. The Y2H screen identified

(D and E) Split-luciferase assay shows the interaction of AvrPm2 with TaZF **(D)** and TaZF homeologs **(E)** in *N. benthamiana*. The red asterisks indicate that $LaCl_3$ treatment was used to suppress TaZF-induced cell death. Co-expression of *CLuc-TaZF* with *NLuc-BgtE-5846*, and *NLuc-AvrPm2* with *CLuc-Pm3B-HA*, served as controls for specific AvrPm2–target interaction. The luminescence signal was measured 3 days post infiltration (dpi). In the plots, data points refer to three independent experiments with six leaf replicates each. For each graph, statistical differences between samples were assessed using non-parametric analysis of variance (Kruskal–Wallis) followed by Dunn's post hoc tests. Samples marked with identical letters in the plot did not differ significantly ($p < 0.05$) in Dunn's test. Median values are indicated by the middle lines in the box plot.

(F) Western blots probed with anti-HA antibodies and anti-luciferase antibodies show protein accumulation of all tested proteins in Y2H and FLuCI experiments, respectively. Expected protein size was 59 kDa for NLuc-tagged effectors, 39 kDa for CLuc-TaZF/CLuc-TaZF_5B/Cluc-TaZF_5D, 43 kDa for CLuc-TaZF_4D, and 207 kDa for CLuc-Pm3B. Expected protein size was 37 kDa for AD-TaZF/AD-TaZF_5B/AD-TaZF_5D and 40 kDa for AD-TaZF_4D. Control refers to untransformed *N. benthamiana* tissue and untransformed yeast cells. Ponceau staining of the western blot membrane is depicted in the lower panels.

Please cite this article in press as: Manser et al., Wheat zinc finger protein TaZF interacts with both the powdery mildew AvrPm2 protein and the corresponding wheat Pm2a immune receptor, Plant Communications (2023), https://doi.org/10.1016/j.xplc.2023.100769

39 candidate host interactors (Supplemental Table 1), among which were two predicted zinc finger proteins, named TaZF_5A (encoded by TraesCS5A01G071900) and TaZF_5D (encoded by TraesCS5D01G084600). TaZF_5A (hereafter called TaZF) is a 188-amino-acid protein that contains a single C2H2 zinc finger motif with a conserved QALGGH sequence in the zinc finger helices and therefore belongs to the C1-1i subclass of Q-type C2H2 zinc finger proteins (Figure 1A) (Ciftci-Yilmaz and Mittler, 2008; Gourcilleau et al., 2011). TaZF also contains a C-terminal ethylene-responsive element-binding factor (ERF)-associated amphiphilic repression (EAR) motif (Ohta et al., 2001) and further belongs to the TFIIIA-type zinc finger proteins (Ciftci-Yilmaz and Mittler, 2008). The second zinc finger protein that interacted with AvrPm2 in the Y2H screen, TaZF_5D, is a close homeolog of TaZF with 97% DNA and 96% amino acid sequence identity. We searched the Chinese Spring wheat reference genome (IWGSC, 2018) for additional *TaZF* homeologs as well as closely related paralogs. In addition to TaZF_5D on chromosome 5D, wheat contains a *TaZF* homeolog on chromosome 5B, *TaZF_5B* (TraesCS5B01G078100), with 96% DNA and 97% amino acid sequence identity (Supplemental Figure 3 and Supplemental Table 2). We also identified three homologs of *TaZF* on chromosome 4, *TaZF_4B* (TraesCS4B01G078400) on chromosome 4B, *TaZF_4D* (TraesCS4D01G077000) on chromosome 4D, and a *TaZF* homolog on chromosome 4A that was not annotated. We therefore predicted a single-exon gene of 687 base pairs, which we refer to here as *TaZF_4A*. The *TaZF* homologs *TaZF_4B*, *TaZF_4D*, and *TaZF_4A* encode proteins with 61%, 59%, and 61% protein sequence identity to TaZF, respectively (Supplemental Figure 3 and Supplemental Table 2).

We investigated whether *TaZF* is expressed under normal conditions and whether gene expression of *TaZF* and its corresponding homeologs and homologs changes after powdery mildew infection. To this end, we compared gene expression in seedlings of the susceptible wheat cultivar Chinese Spring infected with three different *Bgt* isolates (CHE_94202, CHE_96224, and JIW2) with expression in non-infected Chinese Spring. RNA-sequencing data were obtained for three independent biological samples at 2 days post infiltration (dpi) from a previous study (Praz et al., 2018). *TaZF* was expressed in both uninfected and infected wheat. Infected wheat showed lower *TaZF* expression than uninfected wheat, but only infection with isolate 96224 produced a significant difference in *TaZF* expression (Figure 1B). The *TaZF* homeologs *TaZF_5B* and *TaZF_5D* showed similar expression patterns (Supplemental Figure 4A). The *TaZF* homolog *TaZF_4D* was expressed at similar levels under all tested conditions (Supplemental Figure 4A). We also analyzed expression of *TaZF* and its homeologs and homologs in a *Pm2a*-containing wheat line under uninfected and powdery mildew–infected conditions. Initially, we tested whether *Pm2a* expression differed in infected and uninfected tissue, which was not the case (Supplemental Figure 4B). We also observed no changes in expression of *TaZF* and *TaZF* homeologs on chromosome 5 during infection (Supplemental Figure 4C). When we analyzed the expression of *TaZF* homologs on chromosome 4 under infected conditions, we observed a slight upregulation of gene expression compared with uninfected conditions (Supplemental Figure 4D). We concluded that TaZF is constitutively expressed at low levels and that powdery mildew infection causes only minor differences in the expression of *TaZF* and *TaZF* homeologs.

To verify the interaction between AvrPm2 and fragments of TaZF observed in the original Y2H screen, we performed a Y2H assay using the full-length TaZF protein. The GAL4 DNA-binding domain (DBD) and the GAL4 activation domain (AD) were N-terminally fused to AvrPm2 and TaZF, respectively. Yeast growth on selective medium was observed when *DBD-AvrPm2* and *AD-TaZF* were co-expressed (Figure 1C), demonstrating the interaction of their full-length proteins. The interaction between AvrPm2 and TaZF was further tested *in planta* using a split-luciferase assay (Gehl et al., 2011). We generated full-length genes of *AvrPm2* and *TaZF* fused N-terminally to *NLuc* and *CLuc*, respectively. *Agrobacterium tumefaciens*–mediated overexpression of *CLuc-TaZF* itself led to a cell-death response in *N. benthamiana* (Supplemental Figure 2B), which interfered with measurement of the luciferase signal in the interaction assay. We therefore used $LaCl_3$ treatment, which reduced the CLuc-TaZF-induced cell-death response (Supplemental Figure 2B). $LaCl_3$ blocks Ca^{2+} channels at the plasma membrane and thus Ca^{2+} influx, an essential component of the cell-death response (Chen et al., 2017). Co-expression of *CLuc-TaZF* and *NLuc-AvrPm2* in the presence of $LaCl_3$ resulted in a strong luminescence signal (Figure 1D). Co-expression of *CLuc-TaZF* with *NLuc-BgtE-5846*, an AvrPm2 homologous effector (Wicker et al., 2013), in the presence of $LaCl_3$ did not lead to a detectable luminescence signal (Figure 1D), indicating a specific interaction between TaZF and AvrPm2. These results confirmed the results of the Y2H assay and indicated that AvrPm2 interacts with full-length TaZF *in planta*.

In the original Y2H screen, fragments of the TaZF homeolog TaZF_5D interacted with AvrPm2 (Supplemental Table 1), and we wondered whether the full-length homeologous proteins and the other TaZF homologs also interacted with AvrPm2. We therefore tested the TaZF homeologs TaZF_5B and TaZF_5D and the more distant homolog TaZF_4D for interaction with AvrPm2. Because *TaZF_5B*, *TaZF_5D*, and *TaZF_4D* induced cell death when overexpressed in *N. benthamiana* leaves, we used $LaCl_3$ treatment in the split-luciferase assay. TaZF_5B and TaZF_5D, but not TaZF_4D, interacted with AvrPm2 in yeast and *in planta* (Figure 1C and 1E), indicating that the close TaZF homeologs TaZF_5B and TaZF_5D interact with AvrPm2 both in yeast and *in planta*, but the more distantly related TaZF-4D homolog does not. Protein analysis by western blotting demonstrated the presence of all proteins used in the Y2H and split-luciferase experiments (Figure 1F).

Different TaZF amino acid motifs are involved in the interaction with AvrPm2 and the induction of cell death

We investigated which protein parts and amino acid motifs of TaZF are involved in the interaction with AvrPm2. First, we tested whether the integrity of the EAR motif and the QALGGH motif is needed for the interaction of TaZF with AvrPm2. Previous studies on zinc finger proteins have shown that substitution of amino acids in the QALGGH motif causes a loss of DNA-binding ability (Kubo et al., 1998). Therefore, we made TaZF mutants with amino acid substitutions of the alanine ($TaZF^{A78D}$) and the second glycine ($TaZF^{G80D}$) in the QALGGH motif, as well as substitutions ($TaZF^{D183A}$) and deletions (TaZF-ΔEAR) of the EAR motif. Upon overexpression of these mutants in *N. benthamiana* in the absence of $LaCl_3$, we quantified the cell-death response by fluorescence scanning as a proxy for protein functionality. All TaZF

Please cite this article in press as: Manser et al., Wheat zinc finger protein TaZF interacts with both the powdery mildew AvrPm2 protein and the corresponding wheat Pm2a immune receptor, Plant Communications (2023), https://doi.org/10.1016/j.xplc.2023.100769

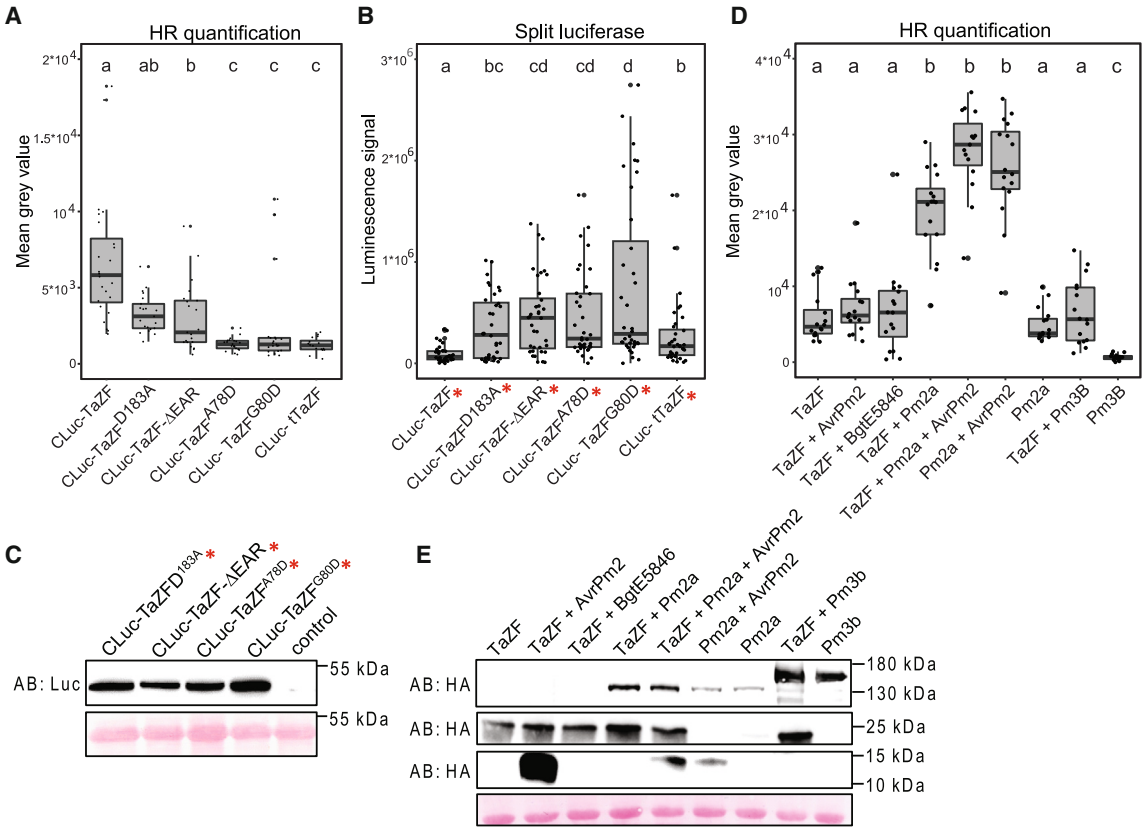

Figure 2. TaZF-induced cell death in *N. benthamiana*, but not the interaction with AvrPm2, is dependent on the integrity of conserved TaZF motifs.

(A) Quantification of cell-death response at 3 dpi in *N. benthamiana* induced by overexpression of *TaZF* mutants with amino acid substitutions in the EAR motif and the QALGGH motif, as well as the truncated *TaZF* mutant tTaZF.

(B) Split-luciferase assay shows the interaction of AvrPm2 and TaZF mutants with amino acid substitutions in the EAR motif and the QALGGH motif, as well as the truncated TaZF mutant tTaZF, in *N. benthamiana*. The red asterisks indicate that $LaCl_3$ treatment was used to suppress TaZF-induced cell death. The luminescence signal was measured at 3 dpi.

(C) Western blots probed with anti-luciferase antibodies show protein accumulation of TaZF mutants N-terminally fused to CLuc at the expected protein size of 39 kDa. Control refers to *N. benthamiana* tissue not expressing *TaZF*. Ponceau staining of the western blot membrane is depicted in the lower panel.

(D) Quantification of the cell-death response in *N. benthamiana* at 3 dpi induced by co-expression of *TaZF* with diverse genes.

(E) Assessment of protein stability by western blot analysis. Protein extracts reflect the co-expression assays in *N. benthamiana* depicted in **(D)**. Expected protein size was 144 kDa for HA-Pm2a, 160 kDa for HA-Pm3b, 21 kDa for HA-TaZF, and 12 kDa for HA-AvrPm2. Antibodies used for western blot analysis are indicated. Ponceau staining of the western blot membrane is depicted in the lower panel.

Data points in **(A)** and **(D)** refer to two independent experiments with seven or eight replicates each. Data points in **(B)** refer to three independent experiments with six leaf replicates each. For each graph, statistical differences between samples were assessed using non-parametric analysis of variance (Kruskal–Wallis) followed by Dunn's post hoc tests. Samples marked with identical letters in the plot did not differ significantly ($p < 0.05$) in Dunn's test. Median values are indicated by the middle lines in the box plot.

mutants showed a reduced cell-death response compared with the wild-type TaZF (Figure 2A); however, $TaZF^{D183A}$ did not cause a significantly lower cell-death response.

When we tested the EAR motif and the QALGGH mutants against AvrPm2 in a split-luciferase assay in the presence of $LaCl_3$, they showed a strongly increased luminescence signal compared with the wild-type TaZF (Figure 2B and 2C). We hypothesize that the increased luminescence signal is due to the reduced cell-death response triggered by TaZF mutants compared with wild-type TaZF. We conclude that the integrity of the EAR motif and the QALGGH motif in TaZF is required for strong cell-death induction in overexpression experiments but not for interaction with AvrPm2.

To further characterize the interaction of TaZF with AvrPm2, we created a truncated TaZF mutant (tTaZF). tTaZF contained the amino acid sequence that was present in all fragments that interacted with AvrPm2 in the initial Y2H screen and that may represent the minimal TaZF sequence necessary for interaction with AvrPm2. The tTaZF mutant is 66 amino acids in length (vs. 188 amino acids for wild-type TaZF) and lacks the N-terminal sequence and the C-terminal domain, including the EAR motif, but it still encodes the DNA-binding QALGGH motif (Figure 1A). Initially, we tested the ability of *tTaZF* to induce cell death upon overexpression in *N. benthamiana*, and in contrast to wild-type *TaZF*, *tTaZF* did not trigger a cell-death response (Figure 2A). When we tested CLuc-tTaZF against NLuc-AvrPm2 in a split-luciferase assay in the presence of $LaCl_3$, we observed strong

Please cite this article in press as: Manser et al., Wheat zinc finger protein TaZF interacts with both the powdery mildew AvrPm2 protein and the corresponding wheat Pm2a immune receptor, Plant Communications (2023), https://doi.org/10.1016/j.xplc.2023.100769

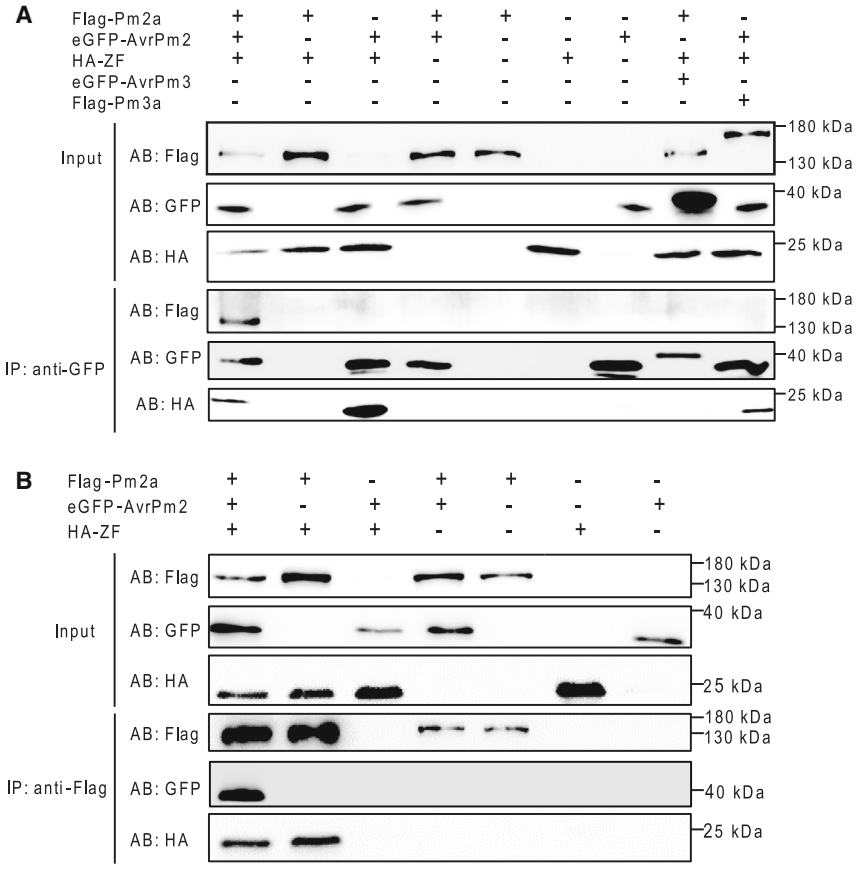

Figure 3. Interaction of Pm2a, TaZF, and AvrPm2 *in planta*.

CoIP experiments with proteins expressed in *N. benthamiana*.

(A) Co-expression of *FLAG-Pm2a*, *eGFP-AvrPm2*, and *HA-TaZF* followed by GFP immunoprecipitation. FLAG-Pm3a and eGFP-AvrPm3b were used as control proteins.

(B) FLAG immunoprecipitation from plant material co-expressing *HA-TaZF* together with *FLAG-Pm2a* and *eGFP-AvrPm2*. Antibodies used for coIP and subsequent detection by western blotting are indicated. Expected protein size was 145 kDa for FLAG-Pm2a, 160 kDa for FLAG-Pm3a, 39 kDa for eGFP-AvrPm2, 41 kDa for eGFP-AvrPm3b, and 21 kDa for HA-TaZF.

luciferase activity, indicating an interaction of CLuc-tTaZF and NLuc-AvrPm2 (Figure 2B). In fact, the luminescence signal was stronger than that of wild-type TaZF (Figure 2B), perhaps owing to the greatly reduced ability of tTaZF to induce cell death. To summarize, a short 66-amino-acid sequence of the TaZF protein (about 30% of the wild-type TaZF protein) containing the DNA-binding QALGGH motif is sufficient for its interaction with AvrPm2.

Given that overexpression of *CLuc-TaZF* in *N. benthamiana* triggers a cell-death response (Figure 2A and Supplemental Figure 2B), we tested wild-type *TaZF* for cell-death induction. Similar to *CLuc-TaZF*, overexpression of wild-type *TaZF* induced a strong cell-death response (Supplemental Figure 2B). Because of the interaction of TaZF with AvrPm2 (Figure 1C and 1D), we hypothesized that co-expression of *TaZF* and *AvrPm2* might affect TaZF-induced cell death. We therefore co-expressed *TaZF* with *AvrPm2* in the absence of $LaCl_3$ and quantified cell death. We also co-expressed *TaZF* with *BgtE-5846*, which did not interact with TaZF in the split-luciferase assay (Figure 1D). TaZF-induced cell death was not modified by co-expression with *AvrPm2* or *BgtE-5846* compared with that induced by TaZF alone (Figure 2D).

Increased TaZF-induced cell death in the presence of Pm2a in *N. benthamiana*

We next tested whether overexpression of *TaZF* together with *Pm2a* affects *TaZF*-induced cell death. Indeed, we observed a strong increase in cell death triggered by co-expression of *TaZF* with *Pm2a* compared with that observed in response to *TaZF* or *Pm2a* alone (Figure 2D). The cell death induced by co-expression of *TaZF* and *Pm2a* was further increased (albeit not significantly) by addition of *AvrPm2*, resulting in a cell-death response comparable to that induced by co-expression of *Pm2a* with *AvrPm2* (Figure 2D). We also co-expressed *TaZF* with *Pm3b*, which did not lead to increased TaZF-induced cell death (Figure 2D). Therefore, we concluded that the cell death induced by overexpression of *TaZF* in *N. benthamiana* is specifically increased by Pm2a.

We wondered whether co-expression of *TaZF*, *Pm2a*, and *AvrPm2* individually or in combination would influence their protein levels, and we therefore performed total protein extractions from co-expression experiments followed by western blot analysis (Figure 2E). TaZF protein levels were not affected by co-expression with *Pm2a* or *AvrPm2* (Figure 2E). Interestingly, co-expression of *Pm2a* together with *TaZF* led to a higher Pm2a protein level compared with that observed after expression of *Pm2a* alone or together with *AvrPm2* (Figure 2E). By contrast, no increased Pm3b protein levels were detectable when *Pm3b was* co-expressed with *TaZF* (Figure 2E), indicating that TaZF specifically stabilizes the Pm2a protein.

AvrPm2 and Pm2a both interact with TaZF *in planta*

The increased TaZF-induced cell death in *N. benthamiana* in the presence of Pm2a suggested an interaction between these two proteins. To test for an interaction between Pm2a, AvrPm2, and TaZF, we performed coIP experiments with transiently transformed *N. benthamiana* leaves. Overexpression of *eGFP-AvrPm2*, *FLAG-Pm2a*, and *HA-TaZF* in *N. benthamiana* indicated the functional integrity of the chimeric proteins (Supplemental Figure 2C). In coIP experiments, eGFP-AvrPm2 interacted with HA-ZF in both the presence and absence of FLAG-Pm2a (Figure 3A). This is consistent with the results of the split-luciferase and Y2H assays (Figure 1) and confirms the interaction of AvrPm2 with TaZF. Interestingly, we observed that FLAG-Pm2a interacted with HA-TaZF in both the presence and absence of AvrPm2 (Figure 3B), suggesting an interaction between FLAG-Pm2a and HA-TaZF. These results indicate that TaZF interacts with both AvrPm2 and Pm2a.

Please cite this article in press as: Manser et al., Wheat zinc finger protein TaZF interacts with both the powdery mildew AvrPm2 protein and the corresponding wheat Pm2a immune receptor, Plant Communications (2023), https://doi.org/10.1016/j.xplc.2023.100769

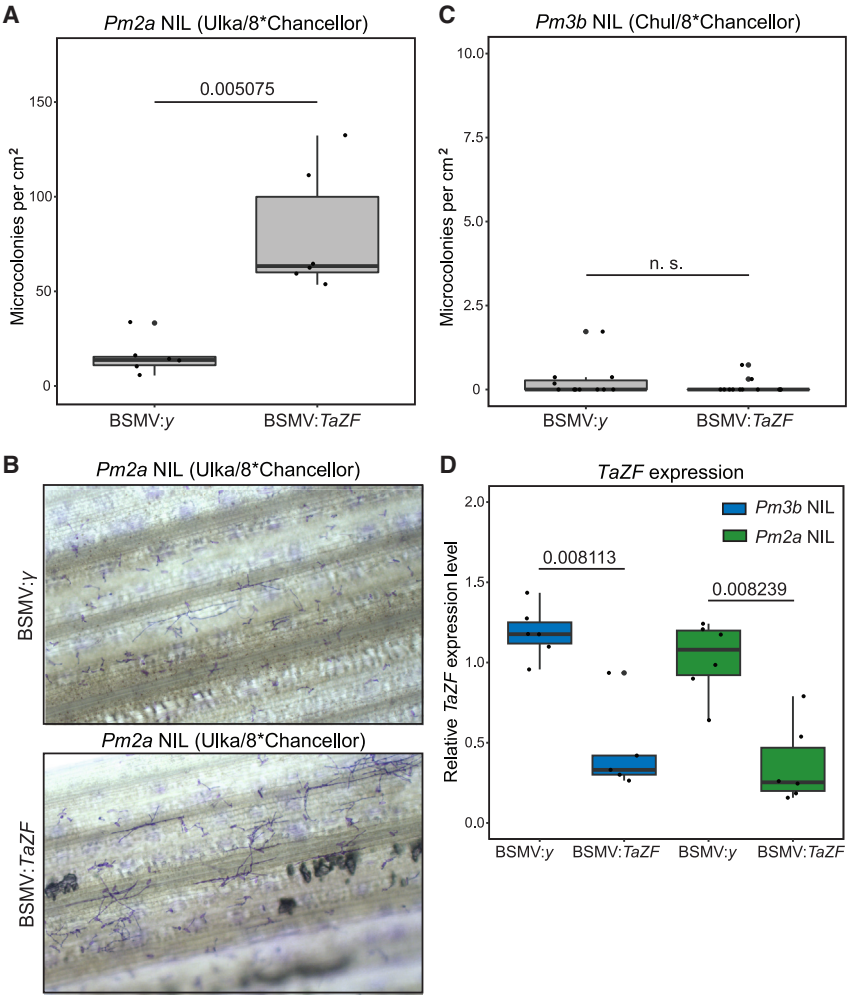

Figure 4. Silencing of *TaZF* in *Pm2a* NIL leads to increased *Bgt* microcolony formation.

(A and C) BSMV-mediated gene silencing (VIGS) of *TaZF* in the wheat *Pm2a* NIL Ulka/8*Chancellor **(A)** and the wheat *Pm3b* NIL Chul/8*Chancellor **(C)**. Inoculation of wheat plants with the wild-type virus (BSMV:γ) served as a negative control. Fourth leaves were infected with the powdery mildew isolate CHE_96224. *Bgt* microcolonies were scored via microscopy. Data points refer to individual leaf segments from one of two independent experiments with a minimum of six replicates each. Median values are indicated by the middle lines in the box plot.

(B) Representative pictures of BSMV:*y*- and BSMV:*TaZF*-silenced *Pm2a* NIL epidermal cells infected with wheat powdery mildew.

(D) *TaZF* expression levels in BSMV:*y*- and BSMV:*TaZF*-silenced *Pm2a* and Pm3b NIL plants assessed by qRT–PCR.

Data points refer to individual plants with a minimum of five replicates each. In each graph, statistical significance was assessed with a two-sided Wilcoxon rank-sum test for unpaired data, and significant *p* values are indicated (n.s., not significant).

Surprisingly, when *eGFP-AvrPm2*, *HA-ZF*, and *FLAG-Pm2a* were transiently expressed together, eGFP-AvrPm2 interacted with FLAG-Pm2a (Figure 3A). In vice versa coIP experiments, FLAG-Pm2a interacted with eGFP-AvrPm2 when *HA-TaZF* was co-expressed (Figure 3B). In contrast to eGFP-AvrPm2, eGFP-AvrPm3b did not interact with HA-ZF and FLAG-Pm2a (Figure 3A). Furthermore, eGFP-AvrPm2 did not interact with FLAG-Pm3a in the presence of TaZF (Figure 3A). Together, these results indicate that Pm2a, TaZF, and AvrPm2 specifically associate with each other *in planta* and that TaZF may act as a stabilizing protein in Pm2a-mediated AvrPm2 recognition, as immunoprecipitation of AvrPm2 by Pm2a and vice versa occurred only in the presence of TaZF. In addition, Pm2a can interact with TaZF also in the absence of AvrPm2, indicating an effector-independent Pm2a–TaZF interaction. Besides the coIP experiments, we did not perform independent experiments to confirm the observation that full-length Pm2a and AvrPm2a interact only in the presence of TaZF, and *TaZF* co-expression had no effect on the Pm2a–LRR domain interaction with AvrPm2a (Figure 6A). We therefore cannot conclude whether the three proteins interact simultaneously or actually form a complex.

Gene silencing of *TaZF* in wheat indicates its involvement in *Pm2a*-mediated powdery mildew resistance

To test whether TaZF and closely related homologs are specifically required for Pm2a-mediated powdery mildew resistance, we performed virus-induced gene silencing (VIGS) of *TaZF* using the barley stripe mosaic virus (BSMV) (Scofield et al., 2005). The VIGS target was designed to cover the 3′ end of *TaZF* and part of the untranslated region (Supplemental Figure 5A). These sequences were predicted to specifically silence *TaZF* and the two homeologs (*TaZF_5B* and *TaZF_5D*) that interacted with AvrPm2 (Figure 1C and 1E) but not *TaZF_4A*, *TaZF_4B*, or *TaZF_4D*. VIGS-mediated silencing of *TaZF* was performed in the two resistant, near-isogenic hexaploid wheat lines Ulka/8*Chancellor (*Pm2a* near-isogenic line [NIL]) and Chul/8*Chancellor (an NIL with the *Pm3b* resistance gene as a control). Infection with the virulent *Bgt* isolate CHE_07004 led to a fully susceptible phenotype in both, wild-type virus BSMV:*y* and BSMV:*TaZF* inoculated plants (Supplemental Figure 5B). We then challenged the BSMV-silenced plants with the avirulent powdery mildew isolate CHE_96224, harboring both *AvrPm2* and *AvrPm3b* (Praz et al., 2017; Bourras et al., 2019). This led to an increase in microcolony and hyphae formation in *TaZF*-silenced *Pm2a* NIL plants compared with *Pm2a* NIL plants infected with the wild-type virus (Figure 4A and 4B). By contrast, we observed similar microcolony formation in *TaZF*-silenced *Pm3b NIL* plants and *Pm3b NIL* plants infected with the wild-type virus BSMV:γ (Figure 4C). Expression analysis by quantitative PCR with reverse transcription (qRT–PCR) showed significantly reduced *TaZF* expression in *Pm2a* and *Pm3b* NIL plants compared with plants inoculated with the wild-type virus (Figure 4D). Furthermore, weak upregulation of *Pm2a* expression was observed in *TaZF*-silenced lines compared with wild-type virus-inoculated plants (Supplemental Figure 5C). Together these results suggest that TaZF is required for Pm2a-mediated, but not Pm3b-mediated, powdery mildew resistance.

Please cite this article in press as: Manser et al., Wheat zinc finger protein TaZF interacts with both the powdery mildew AvrPm2 protein and the corresponding wheat Pm2a immune receptor, Plant Communications (2023), https://doi.org/10.1016/j.xplc.2023.100769

Pm2a, TaZF, and AvrPm2 show nuclear co-localization *in planta*

Given the interaction of Pm2a, TaZF, and AvrPm2 in coIP experiments, we hypothesized that AvrPm2, Pm2a, and TaZF have the same subcellular localization *in planta*. To assess their localization in *N. benthamiana* and wheat, we used the previously generated eGFP-AvrPm2 chimeric protein and also created the protein chimeras TagRFP-TaZF and mTurqois-Pm2a. Functionality testing indicated the functional integrity of the TagRFP-TaZF and mTurqois-Pm2a proteins (Supplemental Figure 2D). In *N. benthamiana*, eGFP-AvrPm2 showed a nucleo-cytoplasmic localization, whereas TagRFP-TaZF localized in the nucleus (Figure 5A) when co-expressed with a cytosolic marker (TagRFP or eGFP). By contrast, mTurqois-Pm2a exclusively localized to the cytoplasm (Figure 5A). We then tested the localization of Pm2a, TaZF, and AvrPm2 in paired combinations. Co-expression of *eGFP-AvrPm2* together with *TagRFP-TaZF* led to nuclear localization of eGFP-AvrPm2 in *N. benthamiana*, whereas localization of TagRFP-TaZF was not affected (Figure 5B). No protein degradation was detected for GFP-AvrPm2, excluding the possibility that the nuclear signal was derived from smaller GFP-containing peptides (Supplemental Figure 6A). Co-expression of *mTurqois-Pm2a* in *N. benthamiana* together with *eGFP-AvrPm2* or *TagRFP-TaZF* led to nuclear localization of mTurqois-Pm2a (Figure 5B). No degradation of mTurqois-Pm2a was detected, excluding the possibility that the nuclear signal was derived from smaller mTurqois-containing peptides (Supplemental Figure 6B). By contrast, co-expression with *mTurqois-Pm2a* did not affect localization of eGFP-AvrPm2 or TagRFP-TaZF, which showed nucleo-cytoplasmic and nuclear localization, respectively (Figure 5B). We then tested the co-localization of all three proteins together and observed that mTurqois-Pm2a, eGFP-AvrPm2, and TagRFP-TaZF co-localized to the nucleus (Figure 5B). TagRFP-TaZF showed an exclusively nuclear localization, whereas eGFP-AvrPm2 and mTurqois-Pm2a showed a nucleo-cytoplasmic localization with a strong nuclear signal (Figure 5B). In summary, Pm2a, AvrPm2, and TaZF co-localized in the nuclear compartment in *N. benthamiana*. A recent study described the localization of Pm2a-GFP, which showed a nucleo-cytoplasmic localization (Jin et al., 2022). However, in contrast to our study, the previous study used a C-terminal fusion of Pm2a to GFP, which may explain the difference in subcellular localization.

We were also interested in the localization of mTurquois-Pm2a, eGFP-AvrPm2, and TagRFP-TaZF proteins in native wheat cells and therefore performed single-cell transformation of wheat leaf epidermal cells by particle bombardment. Similar to their individual localizations in *N. benthamiana*, eGFP-AvrPm2 and TagRFP-TaZF showed a nucleo-cytoplasmic and nuclear localization, respectively (Figure 5C). The TaZF-induced nuclear localization of AvrPm2 that was detected in *N. benthamiana* (Figure 5B) was also observed in wheat (Figure 5D). The localization of mTurqois-Pm2a was not conclusive, as the fluorescence signal of mTurqois-Pm2a was very weak (Figure 5C). In co-bombardments, eGFP-AvrPm2 still showed a nucleo-cytoplasmic localization, whereas the weak mTurqois-Pm2a signal did not improve (Figure 5D). Interestingly, co-bombardment with mTurqois-Pm2a and TagRFP-TaZF led to a stronger mTurqois-Pm2a signal in the nucleus and cytoplasm, whereas TagRFP-TaZF showed a nuclear localization (Figure 5D). Upon co-expression of all three proteins in wheat, mTurqois-Pm2a, eGFP-AvrPm2, and TagRFP-TaZF co-localized in the nucleus (Figure 5D). Similar to results in *N. benthamiana*, mTurqois-Pm2a and eGFP-AvrPm2 showed a nucleo-cytoplasmic localization with a strong nuclear signal, whereas TagRFP-TaZF showed an exclusively nuclear localization (Figure 5D). To summarize, we observed a TaZF-induced shift from nucleo-cytoplasmic to strongly increased nuclear localization of AvrPm2 in both *N. benthamiana* and wheat. In *N. benthamiana*, we observed an increase in the nuclear mTurqois-Pm2a signal when it was co-expressed with *eGFP-AvrPm2* or *TagRFP-TaZF*. In wheat, the signal of mTurqois-Pm2a was very weak when co-bombarded together with a cytosolic marker or eGFP-AvrPm2. However, co-expression of *mTurqois-Pm2a* with *TagRFP-TaZF* led to a strong nucleo-cytoplasmic mTurqois-Pm2a signal, suggesting a TagRFP-TaZF-mediated stabilization of the mTurqois-Pm2a signal. This was consistent with observations from co-expression experiments in *N. benthamiana*, where we found TaZF-mediated stabilization of the Pm2a protein (Figure 2E). Furthermore, we observed nuclear co-localization of mTurqois-Pm2a, eGFP-AvrPm2, and TagRFP-TaZF in *N. benthamiana* and wheat, indicating a nuclear interaction of Pm2a, TaZF, and AvrPm2 *in planta*.

The Pm2a LRR domain mediates the interaction with TaZF

To further characterize the molecular interactions of Pm2a, TaZF and AvrPm2, we investigated whether a single Pm2a domain could mediate the interaction with TaZF and AvrPm2 or whether the full-length Pm2a was required. Previous studies have shown that the LRR domain of NLRs mediates the direct interaction with the effector or with additional components during indirect effector recognition (Wang et al., 2019; Förderer et al., 2022). Therefore, we tested the N-terminally FLAG-tagged LRR domain of Pm2a in coIP experiments in *N. benthamiana* together with eGFP-AvrPm2 and HA-TaZF. In the presence of all three proteins, we observed an interaction of eGFP-AvrPm2 with HA-TaZF and FLAG-LRR (Figure 6A), indicating that the LRR domain of Pm2a domain mediates the interaction with TaZF and AvrPm2. To confirm these results, we assessed the interaction of the Pm2a LRR domain with TaZF in a split-luciferase assay. Indeed, co-expression of *CLuc-LRR* and *NLuc-TaZF* led to a stronger luminescence signal compared with co-expression of *CLuc-LRR* and *NLuc-TaZF* with the control proteins *NLuc-BgtE5846* and *CLuc-BgtE5846*, respectively (Figure 6B), supporting the results of the coIP experiments.

Interestingly, coIP experiments also revealed an interaction of FLAG-LRR with eGFP-AvrPm2 in the absence of HA-TaZF, indicating a direct interaction of AvrPm2 with the LRR domain alone (Figure 6A). We further tested AvrPm2 against the LRR domain in a Y2H assay but could not detect an interaction between the two proteins in this assay (Supplemental Figure 1D). In conclusion, our results suggest that the LRR domain of Pm2a mediates the interaction with TaZF. Furthermore, the Pm2a_LRR domain interacts weakly with AvrPm2 in coIP experiments but not in a Y2H assay.

We previously identified the new AvrPm2-H2 haplotype that differs in two amino acid positions from AvrPm2 and is not recognized by

Please cite this article in press as: Manser et al., Wheat zinc finger protein TaZF interacts with both the powdery mildew AvrPm2 protein and the corresponding wheat Pm2a immune receptor, Plant Communications (2023), https://doi.org/10.1016/j.xplc.2023.100769

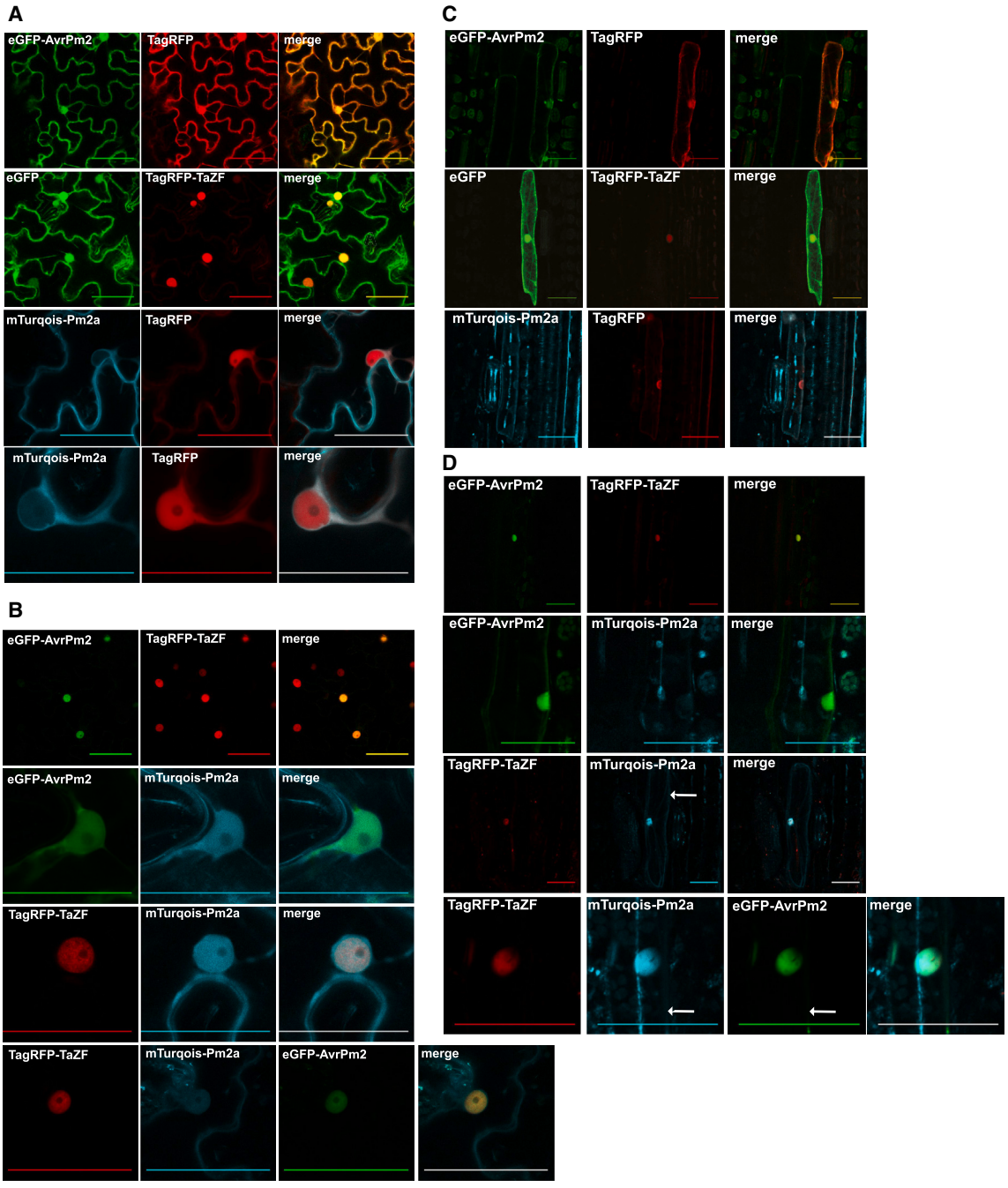

Figure 5. Co-localization of Pm2a, TaZF, and AvrPm2 in *N. benthamiana* and wheat.
Surface views of *N. benthamiana* epidermal cells **(A and B)** and wheat epidermal cells **(C and D)** expressing *eGFP-AvrPm2*, *TagRFP-TaZF*, and *mTurqois-Pm2a* individually together with a cytosolic marker **(A and C)** or in combination **(B and D)**. Pictures were taken by confocal laser scanning microscopy. Free eGFP and TagRFP were used as cytosolic markers. All experiments were repeated two times. White arrows indicate the weak cytosolic signals of mTurqois-Pm2a and eGFP-AvrPm2. Photographs of co-expression are depicted in a row. All scale bars, 60 μm.

Pm2a (Manser et al., 2021). We hypothesized that AvrPm2-H2 does not interact with TaZF because of these polymorphisms and therefore does not trigger a Pm2a-mediated HR. To test this hypothesis, we tested AvrPm2-H2 for interaction with TaZF in split-luciferase and Y2H assays. Indeed, AvrPm2-H2 did not interact with TaZF *in planta* or in yeast (Figure 6C–6E). In coIP experiments, eGFP-AvrPm2-H2 showed a weak interaction with HA-TaZF (Figure 6F) compared with the interaction of eGFP-AvrPm2 with HA-TaZF (Figure 3A). When *FLAG-Pm2a*, *eGFP-AvrPm2-H2*, and *HA-TaZF* were co-expressed, eGFP-AvrPm-H2 did not interact with FLAG-Pm2a and HA-TaZF (Figure 6F). These results indicate that there is a weak interaction of AvrPm2-H2 and TaZF in the absence of Pm2a but, unlike AvrPm2, there is no interaction of Pm2a, TaZF, and AvrPm2-H2 *in planta*. This is likely the reason why AvrPm2-H2 is not recognized by Pm2a and does not trigger Pm2a-mediated HR.

Please cite this article in press as: Manser et al., Wheat zinc finger protein TaZF interacts with both the powdery mildew AvrPm2 protein and the corresponding wheat Pm2a immune receptor, Plant Communications (2023), https://doi.org/10.1016/j.xplc.2023.100769

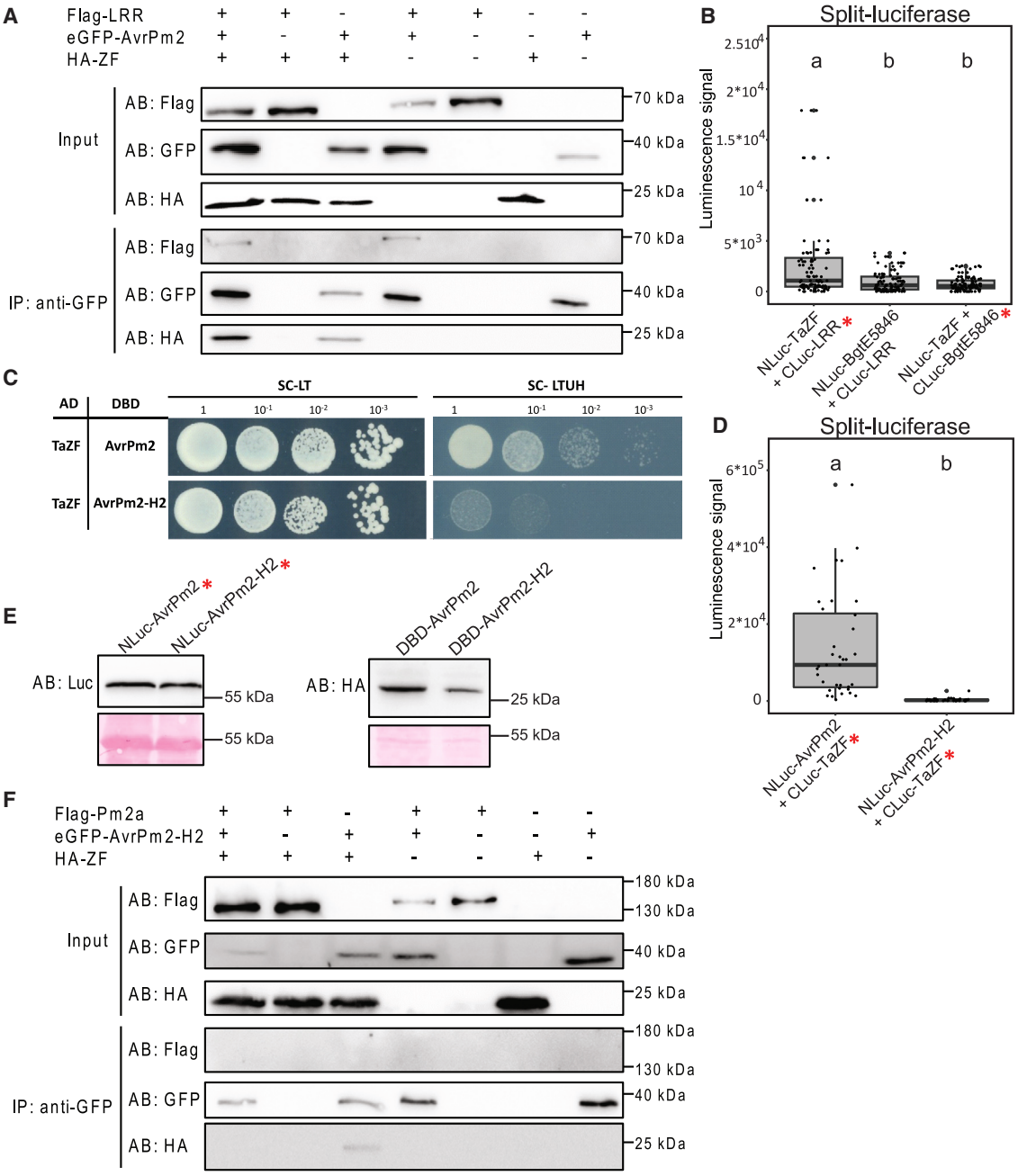

Figure 6. Molecular characterization of the interaction between Pm2a, TaZF, and AvrPm2.

(A and F) CoIP experiments with proteins expressed in *N. benthamiana*. Co-expression of *HA-TaZF* together with *FLAG-LRR* and *eGFP-AvrPm2* **(A)** and together with *FLAG-Pm2a* and *eGFP-AvrPm2-H2* **(F)**, followed by GFP immunoprecipitation. Antibodies used for detection by western blot analysis are indicated. Expected protein size was 145 kDa for FLAG-Pm2a, 70 kDa for FLAG-LRR, 39 kDa for eGFP-AvrPm2/eGFP-AvrPm2-H2, and 21 kDa for HA-TaZF.

(B and D) Split-luciferase assay shows the interaction of TaZF with the Pm2a_LRR domain **(B)** and the lack of interaction of TaZF with AvrPm2-H2 **(D)** in *N. benthamiana*. The red asterisks indicate that $LaCl_3$ treatment was used to suppress TaZF-induced cell death. The luminescence signal was measured at 3 dpi. Data points refer to three independent experiments with six leaf replicates each. For each graph, statistical differences between samples were assessed using non-parametric analysis of variance (Kruskal–Wallis) followed by Dunn's post hoc tests. Samples marked with identical letters in the plot did not differ significantly ($p < 0.05$) in Dunn's test. Median values are indicated by the middle lines in the box plot.

(C) Yeast two-hybrid assay shows no interaction of TaZF with AvrPm2-H2. Photographs were taken after 4 days of incubation and are representative of at least three independent experiments with yeast obtained from three independent yeast transformations.

(E) Western blots show protein accumulation of AvrPm2 variants in FLuCI and Y2H experiments. Expected protein size was 60 kDa for Nluc-AvrPm2 and 31 kDa for DBD-AvrPm2. Antibodies used for western blot analysis are indicated. Ponceau staining of the western blot membrane is depicted in the lower panels.

Please cite this article in press as: Manser et al., Wheat zinc finger protein TaZF interacts with both the powdery mildew AvrPm2 protein and the corresponding wheat Pm2a immune receptor, Plant Communications (2023), https://doi.org/10.1016/j.xplc.2023.100769

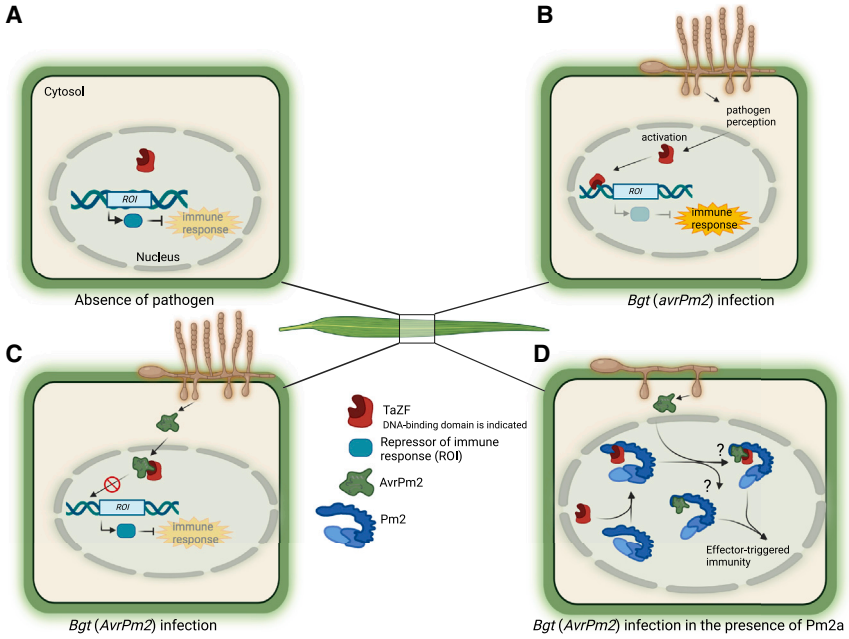

Figure 7. A working model of TaZF as a host target of AvrPm2 and its role in the Pm2a–AvrPm2 interaction.

(A) In the absence of the pathogen, TaZF does not suppress the hypothetical repressor of immune response (*ROI*) gene(s).

(B) Pathogen infection with powdery mildew lacking AvrPm2 leads to activation of TaZF repressor function and to suppression of ROI. Subsequently, immune responses are induced.

(C) In the presence of the pathogen and AvrPm2, AvrPm2 targets TaZF in the nucleus, presumably leading to a disruption of the TaZF repressor function by interfering with the DNA-binding domain. Consequently, ROI is active, and immune responses are repressed.

(D) Pm2a and TaZF form a nuclear pre-activation complex, leading to exposure of the Pm2a_LRR domain. This enables Pm2a–TaZF to bind AvrPm2.

DISCUSSION

We identified the putative wheat transcription factor TaZF, which interacts with both the powdery mildew effector AvrPm2 and the wheat NLR Pm2a. We found that silencing of *TaZF* in wheat led to a reduction in Pm2a-mediated *Bgt* resistance. Upon co-expression of *Pm2a*, *TaZF*, and *AvrPm2*, all three proteins co-localized in the wheat nucleus.

TaZF is a hypothetical repressor of immune signaling and a host target of AvrPm2

TaZF belongs to the TFIIIA-type EAR-motif-containing zinc finger proteins, which are positive regulators of stress responses and are best studied for their roles in biotic and abiotic stress responses (Ohta et al., 2001; Ciftci-Yilmaz and Mittler, 2008; Huang et al., 2012; Yang et al., 2018). The EAR motif is one of the most common transcriptional repression motifs in plants (Kagale and Rozwadowski, 2011; Yang et al., 2018). We found that *TaZF* overexpression led to induction of cell death in *N. benthamiana* (Figure 2A and Supplemental Figure 2B). Previous observations have shown that overexpression of EAR motif-containing proteins from monocots and dicots induce an HR-like cell-death response in tobacco, demonstrating that the cell-death induction processes downstream of EAR-motif-containing proteins are conserved among monocot and dicot plant species (Ogata et al., 2012). Mutants with a deletion of the EAR motif lost the capacity to induce cell death (Ogata et al., 2012). Similarly, TaZF-induced cell death was strongly affected by an amino acid substitution and a deletion of the TaZF EAR motif (Figure 2A), suggesting that this repressor motif is important for cell-death induction in overexpression experiments.

EAR motifs typically mediate the interaction with co-repressors, such as TOPLESS, to form a repressor complex, subsequently leading to transcriptional repression via condensed DNA structure (Kagale and Rozwadowski, 2011; Wu and Citovsky, 2017). It is not known whether TaZF interacts with a wheat homolog of TOPLESS, and specific interaction screens might reveal this homolog. Possibly, the modification or deletion of the EAR motif abolishes the interaction of TaZF with TOPLESS and disrupts the transcriptional repressor function of TaZF, leading to decreased immune responses such as cell death. Mutations in the DNA-binding QALGGH sequence also abolished TaZF-induced cell death (Figure 2A), indicating that DNA binding is necessary for the observed cell-death induction in *N. benthamiana*. Together, these results suggest that TaZF has an active role in transcriptional regulation with a repressor function in the induction of wheat immune responses. We suggest that TaZF is a transcriptional repressor of a hypothetical gene or gene complex in wheat that we call "repressor of immune response" (*ROI*). Expression studies showed that *TaZF* is expressed at similar levels in uninfected and *Bgt*-infected wheat (Figure 1B), indicating that in uninfected plants, TaZF is inactive and might not be able to bind to the *ROI* promoter (Figure 7A). However, pathogen infection leads to TaZF activation, binding of the *ROI* promoter, and subsequent *ROI* suppression, followed by induction of immune responses (Figure 7B). This is in line with previous studies that described the activation of transcription factors after fungal infection, whereupon they play important roles in transcriptional regulation of plant immune responses (Hong et al., 2018). The need for activation of TaZF might be overcome if *TaZF* is overexpressed, resulting in the cell death observed after overexpression of *TaZF* in *N. benthamiana*. We therefore propose that under conditions of overexpression, the correct regulation of the overabundant TaZF proteins fails.

As expected for a predicted transcription factor and observed for other TFIIIA-type zinc finger proteins (Huang et al., 2012), TaZF localized to the plant nucleus (Figure 5). By contrast, AvrPm2 showed a nucleo-cytoplasmic localization, similar to findings in a number of effector localization studies. Most fungal effectors show a cytoplasmic or nucleo-cytoplasmic localization: when expressed in *N. benthamiana*, a majority (43 out of 61) of effectors from the fungal plant pathogen *Colletotrichum higginsianum* showed cytoplasmic or nucleo-cytoplasmic localization (Robin et al., 2018). Interestingly, we observed a strong increase in the

Please cite this article in press as: Manser et al., Wheat zinc finger protein TaZF interacts with both the powdery mildew AvrPm2 protein and the corresponding wheat Pm2a immune receptor, Plant Communications (2023), https://doi.org/10.1016/j.xplc.2023.100769

nuclear AvrPm2 signal upon co-expression with *TaZF* (Figure 5B and 5D), indicating at least a partial TaZF-induced relocalization of AvrPm2. Like that of AvrPm2, a target-dependent localization change was observed for the *Bgh* effectors CSEP0105 and CSEP0162, which show cytosolic and nuclear localization in barley epidermal cells. Co-expression of the effectors with their host targets resulted in exclusive accumulation of CSEP0105 and CSEP0162 in the cytosol (Ahmed et al., 2015).

Given the active role of TaZF in transcriptional regulation and the TaZF-induced increase in nuclear AvrPm2 localization, we hypothesize that TaZF is the host target of AvrPm2. Transcriptional regulation mediated by the TOPLESS transcriptional repressor in complex with EAR-motif-containing transcription factors has previously been reported to be a host target of filamentous pathogens. The *Ustilago maydis* effector Jsi1 and the downy mildew effector HaRxL21 both contain an EAR motif with which they bind to the maize and *Arabidopsis* co-repressor Topless and Topless-related proteins (TPL/TRPs), respectively (Harvey et al., 2020; Darino et al., 2021). By binding to TPL/TPRs via the EAR motif, Jsi1 blocks the formation of an ethylene response factor (EFR)–TPL/TPR complex, leading to ethylene signaling and subsequently to susceptibility to biotrophic pathogens (Darino et al., 2021). By contrast, AvrPm2 does not contain an EAR motif but interacts with the EAR-motif-containing TaZF in wheat and thereby possibly targets transcriptional regulation mediated by the TOPLESS repressor complex. Deletion of the TaZF–EAR motif did not affect the interaction with AvrPm2 (Figure 2B), suggesting that AvrPm2 does not interact with TaZF through the EAR motif and that the hypothetical TaZF–TOPLESS complex formation is not affected. Instead, a small 66-amino-acid fragment of the TaZF protein, containing the DNA-binding QALGGH motif but lacking the EAR motif, was sufficient for the interaction with AvrPm2 (Figure 2B). Substitution of single amino acids in the QALGGH motif did not affect the interaction of TaZF with AvrPm2 (Figure 2B), suggesting that the integrity of the QALGGH motif and DNA binding are dispensable for the interaction with AvrPm2. Interaction of AvrPm2 with TaZF may therefore occur through amino acid motifs surrounding the QALGGH sequence (Figure 7C), and AvrPm2 possibly interferes with the DNA-binding activity of TaZF, leading to disruption of the transcriptional repression of *ROI* by TaZF. The *ROI* gene product would then be produced, and immune responses would be inhibited (Figure 7C). It is also possible that the interaction of AvrPm2 interferes with the proposed activation of TaZF, which is needed for exertion of its repressor function. To summarize, we propose that binding of AvrPm2 to TaZF disrupts the ability of TaZF to form complexes with host DNA or other host proteins and thereby leads to modified transcriptional regulation of wheat immune responses. This is in line with previous studies, which did not describe enzymatic activity for most characterized effectors from filamentous pathogens, and suggests that these effectors instead disrupt the formation of biologically active protein complexes to subvert immunity (He et al., 2020; Saur et al., 2021).

Is there direct or indirect effector recognition through TaZF involvement in Pm2a-mediated AvrPm2 recognition?

We found that the wheat NLR Pm2a and TaZF interact independently of the presence of AvrPm2, suggesting a nuclear preactivation complex, and that the LRR domain of Pm2a is sufficient for interaction with AvrPm2. However, we did not detect interaction of full-length Pm2a with AvrPm2 in the Y2H assay, and we cannot exclude the possibility of indirect effector recognition of AvrPm2 by Pm2a in which TaZF acts as a scaffold for both the effector and the NLR (Figure 7D). There could be a homologous zinc finger protein with a conserved function in *N. benthamiana* (NbZF) that mediates the interaction between heterologously expressed *Pm2a* and *AvrPm2*, thus leading to HR. The TaZF homolog NbZF might, like TaZF (Figure 1B), have low expression levels, and a low amount of NbZF protein might therefore be present in *N. benthamiana*. This would still be sufficient to mediate interaction between Pm2a and AvrPm2, leading to Pm2a activation and subsequent cell death. NbZF proteins might also be present in coIP experiments mediating the AvrPm2–Pm2a interaction, although at low amounts.

Alternatively, recognition of AvrPm2 by Pm2a might be based on an exclusively direct interaction. Using truncated Pm2a constructs, we found that the LRR domain of Pm2a mediates the interaction with TaZF *in planta*. The LRR domain also interacted with AvrPm2 in coIP experiments (Figure 6A and 6B) but not in Y2H experiments (Supplemental Figure 1D). Full-length Pm2a did not directly interact with AvrPm2, although we used experimental approaches that were successful in demonstrating the direct interaction between MLA13 and Avra13_V2 (Figure 3A and 3B; Supplemental Figure 1). We suggest that there are contact points between AvrPm2 and the LRR domain and that there is a direct, albeit weak and transient, AvrPm2–LRR interaction. This interaction might be too weak to detect using full-length Pm2a and AvrPm2 in protein interaction assays, or the LRR interaction sites in the full-length Pm2a protein may not be sufficiently accessible to AvrPm2. We hypothesize that transient binding of TaZF to Pm2a leads to conformational changes in Pm2a, exposing the LRR domain, which can then interact stably with AvrPm2 (Figure 7D). TaZF would thus act as a facilitator of the Pm2a–AvrPm2 interaction.

We demonstrated that the virulent AvrPm2-H2 haplovariant (Manser et al., 2021) does not interact with TaZF and Pm2a (Figure 6), suggesting that there is no interaction of Pm2a, TaZF, and AvrPm2-H2 (Figure 6F). We suggest that the two polymorphisms between AvrPm2 and AvrPm2-H2 prevent binding of AvrPm2-H2 to TaZF. This causes a loss of effector–target interaction but also, at the same time, an evasion of Pm2a-mediated effector recognition of AvrPm2-H2.

Localization and function of Pm2a, TaZF, and AvrPm2

We found that Pm2a was localized in the cytosol in *N. benthamiana,* whereas the Pm2a signal was very weak in wheat. Co-expression of *Pm2a* with *TaZF* led to elevated Pm2a protein levels (Figure 2E) and a nucleo-cytosolic Pm2a signal in *N. benthamiana* (Figure 5B). Furthermore, co-expression of *Pm2a* with *TaZF* in wheat led to a strong Pm2a signal in the nucleus and cytoplasm (Figure 5D), suggesting TaZF-mediated stabilization of the Pm2a protein. Co-localization experiments with all three proteins showed a TaZF-induced increase in nuclear Pm2a and AvrPm2 signals and an exclusively nuclear signal of TaZF (Figure 5B and 5D), suggesting the nuclear localization of all three components, Pm2a–TaZF–AvrPm2 (Figure 7D). Nuclear localization has been described for other plant NLRs, which interact with transcription factors. The barley immune receptor MLA10 shows nucleo-cytoplasmic localization in barley cells (Shen et al., 2007), and there is a direct

Please cite this article in press as: Manser et al., Wheat zinc finger protein TaZF interacts with both the powdery mildew AvrPm2 protein and the corresponding wheat Pm2a immune receptor, Plant Communications (2023), https://doi.org/10.1016/j.xplc.2023.100769

interaction between Mla10 and Avra10 (Saur et al., 2019). MLA10 interacts with the transcriptional repressor HVWRKY2 and thereby possibly derepresses PAMP-triggered basal defense (Shen et al., 2007). Decreasing the nuclear MLA10 concentration leads to decreased *Bgh* resistance and increased cell-death induction. Exclusive nuclear localization of MLA10 led to increased *Bgh* resistance, and cell-death induction was abolished (Shen et al., 2007; Bai et al., 2012). Therefore, a dual role of MLA10 in a compartment-dependent manner was suggested, which includes an uncoupling of nuclear disease resistance signaling from cytosolic cell-death induction (Shen et al., 2007). The cytosolic fraction of the tobacco NLR N, together with NRIP1, recognizes the helicase domain (p50) of the tobacco mosaic virus, whereas the nuclear N fraction interacts with the plant homeodomain-containing transcriptional repressor AL7 (Caplan et al., 2008; Zhang et al., 2023). Upon virus infection, AL7 is phosphorylated, which impairs its interaction with the N immune receptor and leads to release of AL7 from N. Free, phosphorylated AL7 can bind to the promoters of genes related to reactive oxygen species (ROS) scavenging, leading to their suppression and subsequently creating a favorable environment for ROS accumulation (Zhang et al., 2023). Knockout of *AL7* led to compromised N-mediated viral resistance, similar to the silencing of *TaZF*, which impaired Pm2a-mediated *Bgt* resistance. Thus, a transcriptional repressor positively regulates NLR-mediated resistance by repressing negative regulators of immune signaling (Zhang et al., 2023). Co-expression of *TaZF* together with *Pm2a* strongly increased *TaZF*-induced cell death (Figure 2D). Assuming that TaZF is a transcriptionally active repressor (Figure 7A and 7B), we propose that Pm2a positively affects the transcriptional activity of TaZF. Hence, overabundance of both proteins leads to Pm2a-mediated activation of TaZF and subsequently to immune responses and cell death. We propose a model in which Pm2a recognizes AvrPm2 through binding of AvrPm2 to the Pm2a–TaZF pre-activation complex leading to NLR activation (Figure 7D). Based on earlier findings on MLA10 and N, we suggest that nuclear localization determines effector-triggered immune responses through activation of TaZF's transcriptional repressor function by Pm2a. It is unclear whether a small cytosolic fraction of activated Pm2a forms a resistosome-like structure involved in the induction of cell death.

To conclude, we identified TaZF as an interactor of both Pm2a and AvrPm2 and as a third component that may possibly contribute to Pm2a-mediated AvrPm2 recognition. This demonstrates the importance of studying effector host targets for the understanding of Avr–NLR interactions. We suggest that the wheat NLR Pm2a provides a link between effector-based pathogen detection and transcriptional processes that coordinate immune responses. Future work should focus on identification of the transcriptional targets of TaZF and/or the Pm2a–TaZF complex and on the underlying mechanism by which Pm2a-mediated effector recognition leads to transcriptional regulation of wheat defense responses.

METHODS

Yeast two-hybrid analysis

The initial Y2H screen was performed by Hybrigenics Services (https://www.hybrigenics-services.com). AvrPm2 without a signal peptide (Supplemental Table 3) was used as a bait against a cDNA prey library from hexaploid wheat inoculated with the hemibiotrophic fungal wheat pathogen *Zymoseptoria tritici* (library reference: WLIZT).

The ProQuest Two-Hybrid System was used for Y2H experiments (Invitrogen, Waltham, MA, USA). Genes of interest (Supplemental Table 3) with an N-terminal HA tag were cloned into the bait plasmid pDEST22 and into the prey plasmid pDEST32. The yeast strain MaV203 was co-transformed with bait and prey plasmids, and transformants were selected on medium lacking leucine and tryptophan (SC-LT). Co-transformations with empty pDEST22 and pDEST32 served as controls. Single colonies were selected and grown in liquid SC-LT overnight before harvest of the cells and adjustment of the OD_{600} to 1 in 1× Tris–EDTA buffer (10 mM Tris–HCl, 1 mM EDTA [pH 7.5]). A dilution series from OD_{600} = 1 to OD_{600} = 0.001 was created and placed on SC-LT medium and on medium without leucine, tryptophan, histidine, and uracil (SC-LTUH).

Split-luciferase assay

For the *in vitro* luciferase complementation assay in *N. benthamiana*, genes of interest (Supplemental Table 3) were cloned into the FLuCI plasmids pDEST-NIuc-GW and pDEST-CLuc-GW (Gehl et al., 2011). *A. tumefaciens* strain GV3101 harboring NLuc and CLuc constructs were mixed in a (1:1):1 ratio with the *A. tumefaciens* p19-silencing-suppressor strain (Jay et al., 2023) prior to infiltration into *N. benthamiana* plants. Transient expression by agroinfiltration in *N. benthamiana* was performed as described previously (Bourras et al., 2015). Plants expressing *TaZF* constructs were infiltrated with 2 mM $LaCl_3$ 16 h after initial *A. tumefaciens* infiltration to suppress the cell death induced by *TaZF* (Chen et al., 2017). After 3–4 dpi, two leaf disks (6-mm diameter) were collected from each leaf and incubated in buffer (10 mM MES–KOH [pH 5.6], 10 mM $MgCl_2$). Leaf disks were incubated in darkness for 10 min, and 1 mM luciferin (BioVision, Milpitas, CA, USA) in 0.5% DMSO was added. The luciferase luminescence signal was immediately imaged for 25 min using the Spark imaging system (Tecan, Männedorf, Switzerland).

Protein extraction and western blot analysis

For total protein extraction, yeast strains were grown in 8 ml of SC-LT liquid medium at 28°C overnight. Cells were harvested by centrifugation for 5 min at 700 *g*, and the pellet was washed with 1 mM EDTA. The pellet was resuspended in 200 μl of NaOH and incubated on ice for 10 min; 200 μl of 50% trichloroacetic acid (TCA) was then added, and the sample was incubated on ice for 60 min. After centrifugation for 20 min at 14 000 *g*, the pellet was washed with 200 μl of acetone. The pellet was resuspended in 200 μl of 5% SDS, and 200 μl of 1× Laemmli sample buffer was added. The sample pH was adjusted to 4.6 with 1 M Tris (pH 10), and the sample was incubated at 37°C for 15 min with shaking. After centrifugation for 15 min at 14 000 *g*, the supernatant was collected.

N. benthamiana tissue for total protein extraction was harvested 2–3 dpi from four independent leaves by collecting two leaf disks per leaf. The tissue was immediately frozen in liquid nitrogen and ground with a pestle. The sample was heated in 150 μl SDS sample buffer for 10 min at 95°C. Samples were centrifuged twice for 5 min at 15 000 *g*, and the supernatants were collected.

Total protein samples were separated on an SDS–PAGE gel and transferred to a nitrocellulose membrane (GE Healthcare, Chicago, IL, USA). Membranes were probed with monoclonal horseradish peroxidase (HRP)-conjugated anti-HA antibodies (Roche, Basel, Switzerland) or primary unconjugated, polyclonal rabbit anti-luciferase antibodies (Sigma-Aldrich, St. Louis, MO, USA) followed by HRP-conjugated anti-rabbit antibodies (LabForce, Muttenz, Switzerland). Antibodies were detected by HRP activity on westernBright ECL HRP substrate (Advansta, San Jose, CA, USA) using the Fusion FX system (Vilber Lourmat, Eberhardzell, Germany).

Cell-death quantification

N. benthamiana were infiltrated with the desired constructs. Induced cell death was measured at 2–3 dpi by fluorescence scanning of the abaxial sides of leaves as described previously (Praz et al., 2017). Cell death

Please cite this article in press as: Manser et al., Wheat zinc finger protein TaZF interacts with both the powdery mildew AvrPm2 protein and the corresponding wheat Pm2a immune receptor, Plant Communications (2023), https://doi.org/10.1016/j.xplc.2023.100769

was quantified with ImageJ software by measuring the mean gray value of the infiltrated area. Experiments were repeated two times with eight replicates each time.

Co-immunoprecipitation

To avoid cell death induced by overexpression of *TaZF*, *Pm2a*, and *AvrPm2*, *Agrobacteria*-infiltrated *N. benthamiana* tissue was harvested 44 h post infiltration (hpi) and immediately flash-frozen in liquid nitrogen. Leaf material (250 mg) was ground to a fine powder and resuspended in 1.25 ml of extraction buffer (150 mM Tris–HCl [pH 7.5], 150 mM NaCl, 10% glycerol, 1 mM EDTA, 10 mM dithiothreitol, 0.5% Triton X-100, 1 mM phenylmethylsulfonyl fluoride, and protease inhibitor). The suspension was incubated with rotation for 30 min at 4°C, followed by two centrifugation steps at 21 000 *g* for 20 min at 4°C. The supernatant was incubated with 15 μl of prewashed anti-FLAG (Thermo Fisher, Waltham, MA, USA) or 10 μl of prewashed anti-GFP (Chromotek, Planegg, Germany) magnetic beads for 5.5 h at 4°C with rotation. The beads were washed five times with extraction buffer and boiled in 60 μl of 1× Laemmli sample buffer for 10 min at 95°C. Proteins from crude extracts (input) and precipitated proteins were detected by western blot analysis with HRP-conjugated anti-GFP (Biolegend, San Diego, CA, USA), anti-FLAG (Sigma-Aldrich), or anti-HA (Roche) antibodies.

Virus-induced gene silencing

The designed target with flanking restriction sites (Supplemental Figure 5) was synthesized by GeneArt (Thermo Fisher) and cloned in the antisense direction into the pBS-BSMV-γ plasmid. The wild-type viral genome (pBS-BSMV-γ) was used as a negative control. VIGS was performed as described previously (Scofield et al., 2005; Bhullar et al., 2009). The viral RNA was synthesized *in vitro* with the mMESSAGE mMACHINE T7 Transcription Kit (Thermo Fisher). Similar amounts of pBS-BSMV-α, pBS-BSMV-β and pBS-BSMV-TaZF and pBS-BSMV-γ, respectively were used to inoculate the fully expanded first leaf of 9-day-old *Pm2a*-containing Ulka/8*Chancellor seedlings (Parlange et al., 2015; Sánchez-Martín et al., 2016) and *Pm3b*-containing Chul/8*Chancellor seedlings. Fourteen days after inoculation, the fourth leaves were detached, and 25 mg of leaf material was collected for qRT–PCR analysis, shock-frozen in liquid nitrogen, and stored at −80°C. The leaf base of the fourth leaf was placed on 0.5% agar plates containing 10 g/l 6-benzylaminopurine and infected with the avirulent Swiss *Bgt* isolate CHE_96224 harboring *AvrPm2* and *AvrPm3b* or with the virulent Swiss Bgt isolate CHE_07004 (Praz et al., 2017; Lindner et al., 2020). After 72 h, leaves infected with the virulent isolate were destained for 3 days (16.6% glycerol, 8.3% lactic acid in ethanol). To detect fungal spores and hyphae from infections with the avirulent isolate, the destained leaves were stained with Coomassie brilliant blue (0.2% in ethanol), washed with water, and stored in 60% glycerol. The microcolonies were counted on the fourth leaf using a conventional bright-field microscope.

qRT–PCR analysis of *TaZF* and *Pm2a* gene expression

Leaf material of uninfected and CHE_07004-infected Ulka/8*Chancellor wheat lines was sampled at 72 hpi, shock-frozen in liquid nitrogen, and stored at −80°C.

RNA extraction was performed with the Dynabeads mRNA DIRECT Purification Kit (61012, Invitrogen) according to the manufacturer's protocol with the following modifications. Lysis was performed in 600 μl, 300 μl of which was used with 12 μl of oligo$(dT)_{25}$ per extraction. Binding, washing, and elution were performed using the KingFisher Apex Purification System (Thermo Fisher) in 96 deep-well blocks. First-strand cDNA was synthesized from 20 ng of mRNA, including a double-stranded DNase digest, with Maxima H Minus cDNA Synthesis Master Mix (M1682, Thermo Scientific) in a total reaction volume of 6 μl.

Expression of *TaZF* and *Pm2a* was assessed by qRT–PCR on a CFX Opus 96 thermal cycler (Bio-Rad) following the MIQE guidelines (Bustin et al., 2009). Two reference genes, *ADP* and *Ta6863*, were selected for normalization (Giménez et al., 2011; Hurni et al., 2013). Specificities of amplicons, RT-minus control check, melting curve assessment, and efficiency calculation were performed as described previously (Hurni et al., 2015). Target-specific amplification efficiencies and primer sequences for all targets are given in Supplemental Table 4. Primer pairs were selected to detect the combined expression levels of *TaZF* and *TaZF* homeologs on chromosome 5 and *TaZF* homologs on chromosome 4 (Supplemental Table 4).

qRT–PCR was performed as described previously (Sánchez-Martín et al., 2021). Thermocycling conditions were 95°C for 20 s, followed by 40 cycles of 95°C for 3 s and 60°C for 20 s for all targets. A subsequent melting curve assessment was performed to exclude detection of potential primer dimers. Relative quantities were calculated and normalized to the reference genes *ADP* and *Ta6863* to obtain calibrated normalized relative expression values using CFX Maestro software (Bio-Rad).

Amplicon sequencing to detect differential expression of *TaZF* homeologs and homologs

To differentiate the expression of individual *TaZF* homeologs and homologs on chromosomes 4 and 5, respectively, conserved primers were designed to amplify all three *TaZF* copies per chromosome (Supplemental Table 5). PCR was performed using Phusion High-Fidelity polymerase (M0530, NEB) according to the manufacturer's protocol with 4 μl of cDNA in a 40-μl reaction volume at an annealing temperature of 60°C with 36 cycles. Amplicons were purified with the E.Z.N.A. Cycle-Pure Kit (D6492-02, Omega Bio-Tek). The purified product (200 ng) was sent to Plasmidsaurus (Eugene, OR, USA) for amplicon sequencing. Adaptor-trimmed single reads were mapped to the reference sequences of *TaZF* and *TaZF* homeologs on chromosome 5 and *TaZF* homologs on chromosome 4. Reads mapped to regions that contained distinctive polymorphisms between the A, B, and C genome versions were counted for each copy individually to assess differential expression, if any.

Subcellular protein localization in *N. benthamiana* and wheat via confocal laser scanning microscopy

For subcellular protein localization studies, *AvrPm2* and *TaZF* were cloned into pGWB506 (N-terminal *eGFP* fusion) and pGWB235 (N-terminal *TagRFP* fusion) (Nakagawa et al., 2007), respectively. An N-terminal fusion was used to fuse *Pm2a* to *mTurqois* in pIPKb004 (for localization studies in *N. benthamiana*) or pIPKb002 (for localization studies in wheat) (Himmelbach et al., 2007). *A. tumefaciens* harboring eGFP constructs, TagRFP constructs, and mTurqois constructs were mixed with the p19 strain (Jay et al., 2023) prior to infiltration into *N. benthamiana* plants. The *N. benthamiana* plants were incubated for 2 days.

Particle bombardment of single wheat epithelial cells was performed as described previously (Brunner et al., 2010). Leaf segments of primary leaves from 10-day-old plants of the wheat cultivar Chancellor were co-bombarded with 6 μg of total DNA. Leaf segments were incubated for 48 h at 20°C and 80% relative humidity.

Confocal images of *N. benthamiana* tissue were taken using a Leica SP5 confocal laser scanning microscopy system (Leica, Wetzlar, Germany) equipped with an argon laser (488 nm) and a DPSS561 laser (561 nm). Emission of mTurqois was collected at 465–490 nm, emission of eGFP was collected at 510–530 nm, and emission of TagRFP was collected at 570–590 nm. Confocal images of bombarded wheat leaves were taken using a Leica SP5 or SP8 confocal laser scanning microscopy system, later equipped with an argon laser (458 nm) and a white laser (554 nm). Emission of mTurqois, eGFP, and TagRFP was collected at 465–490 nm, 491–572 nm, and 570–600 nm, respectively.

SUPPLEMENTAL INFORMATION

Supplemental information is available at *Plant Communications Online*.

FUNDING

This work was supported by grants from the Swiss National Science Foundation (310030_204165 and 310030B_182833) and by funding from the University of Zurich.

AUTHOR CONTRIBUTIONS

B.M., H.Z., G.H., J.S., J.I., and S.B. performed experiments. B.M., H.Z., G.H., S.B., T.W., and B.K. analyzed the data and interpreted the results. B.M. and B.K. designed the project and wrote the manuscript.

ACKNOWLEDGMENTS

We thank Jaruschka Pecnik and Steven Zwartkruis for technical assistance. No conflict of interest is declared.

Received: August 1, 2023
Revised: November 2, 2023
Accepted: November 15, 2023

REFERENCES

Ahmed, A.A., Pedersen, C., Schultz-Larsen, T., Kwaaitaal, M., Jørgensen, H.J.L., and Thordal-Christensen, H. (2015). The Barley Powdery Mildew Candidate Secreted Effector Protein CSEP0105 Inhibits the Chaperone Activity of a Small Heat Shock Protein. Plant Physiol. **168**:321–333.

Bai, S., Liu, J., Chang, C., Zhang, L., Maekawa, T., Wang, Q., Xiao, W., Liu, Y., Chai, J., Takken, F.L.W., et al. (2012). Structure-Function Analysis of Barley NLR Immune Receptor MLA10 Reveals Its Cell Compartment Specific Activity in Cell Death and Disease Resistance. PLoS Pathog. **8**, 1002752.

Bauer, S., Yu, D., Lawson, A.W., Saur, I.M.L., Frantzeskakis, L., Kracher, B., Logemann, E., Chai, J., Maekawa, T., and Schulze-Lefert, P. (2021). The leucine-rich repeats in allelic barley MLA immune receptors define specificity towards sequence-unrelated powdery mildew avirulence effectors with a predicted common RNase-like fold. PLoS Pathog. **17**, e1009223.

Bhullar, N.K., Street, K., Mackay, M., Yahiaoui, N., and Keller, B. (2009). Unlocking wheat genetic resources for the molecular identification of previously undescribed functional alleles at the Pm3 resistance locus. Proc. Natl. Acad. Sci. USA **106**:9519–9524.

Bourras, S., McNally, K.E., Ben-David, R., Parlange, F., Roffler, S., Praz, C.R., Oberhaensli, S., Menardo, F., Stirnweis, D., Frenkel, Z., et al. (2015). Multiple Avirulence Loci and Allele-Specific Effector Recognition Control the Pm3 Race-Specific Resistance of Wheat to Powdery Mildew. Plant Cell **27**:2991–3012.

Bourras, S., Kunz, L., Xue, M., Praz, C.R., Müller, M.C., Kälin, C., Schläfli, M., Ackermann, P., Flückiger, S., Parlange, F., et al. (2019). The AvrPm3-Pm3 effector-NLR interactions control both race-specific resistance and host-specificity of cereal mildews on wheat. Nat. Commun. **10**:2292.

Boutrot, F., and Zipfel, C. (2017). Function, Discovery, and Exploitation of Plant Pattern Recognition Receptors for Broad-Spectrum Disease Resistance. Annu. Rev. Phytopathol. **55**:257–286.

Brunner, S., Hurni, S., Streckeisen, P., Mayr, G., Albrecht, M., Yahiaoui, N., and Keller, B. (2010). Intragenic allele pyramiding combines different specificities of wheat Pm3 resistance alleles. Plant J. **64**:433–445.

Bustin, S.A., Benes, V., Garson, J.A., Hellemans, J., Huggett, J., Kubista, M., Mueller, R., Nolan, T., Pfaffl, M.W., Shipley, G.L., et al. (2009). The MIQE Guidelines: Minimum Information for Publication of Quantitative Real-Time PCR Experiments. Clin. Chem. **55**:611–622.

Cao, Y., Kümmel, F., Logemann, E., Gebauer, J.M., Lawson, A.W., Yu, D., Uthoff, M., Keller, B., Jirschitzka, J., Baumann, U., et al. (2023). Structural polymorphisms within a common powdery mildew effector scaffold as a driver of coevolution with cereal immune receptors. Proc. Natl. Acad. Sci. USA **120**, e2307604120.

Caplan, J.L., Mamillapalli, P., Burch-Smith, T.M., Czymmek, K., and Dinesh-Kumar, S.P. (2008). Chloroplastic Protein NRIP1 Mediates Innate Immune Receptor Recognition of a Viral Effector. Cell **132**:449–462.

Cesari, S. (2017). Multiple strategies for pathogen perception by plant immune receptors. In New Phytol (Advance Access).

Chen, T., Liu, D., Niu, X., Wang, J., Qian, L., Han, L., Liu, N., Zhao, J., Hong, Y., and Liu, Y. (2017). Antiviral resistance protein Tm-22 functions on the plasma membrane. Plant Physiol. **173**:2399–2410.

Chen, J., Zhang, X., Rathjen, J.P., and Dodds, P.N. (2022). Direct recognition of pathogen effectors by plant NLR immune receptors and downstream signalling. Essays Biochem. **66**:471–483.

Ciftci-Yilmaz, S., and Mittler, R. (2008). The zinc finger network of plants. Cell. Mol. Life Sci. **65**:1150–1160.

Darino, M., Chia, K.S., Marques, J., Aleksza, D., Soto-Jiménez, L.M., Saado, I., Uhse, S., Borg, M., Betz, R., Bindics, J., et al. (2021). Ustilago maydis effector Jsi1 interacts with Topless corepressor, hijacking plant jasmonate/ethylene signaling. New Phytol. **229**:3393–3407.

Dean, R., Van Kan, J.A.L., Pretorius, Z.A., Hammond-Kosack, K.E., Di Pietro, A., Spanu, P.D., Rudd, J.J., Dickman, M., Kahmann, R., ELLIS, J., and Foster, G.D. (2012). The Top 10 fungal pathogens in molecular plant pathology. Mol. Plant Pathol. **13**:414–430.

Dodds, P.N., Lawrence, G.J., Catanzariti, A.-M., Teh, T., Wang, C.-I.A., Ayliffe, M.A., Kobe, B., and Ellis, J.G. (2006). Direct protein interaction underlies gene-for-gene specificity and coevolution of the flax resistance genes and flax rust avirulence genes. Proc. Natl. Acad. Sci. USA **103**:8888–8893.

Duxbury, Z., Ma, Y., Furzer, O.J., Huh, S.U., Cevik, V., Jones, J.D.G., and Sarris, P.F. (2016). Pathogen perception by NLRs in plants and animals: Parallel worlds; Pathogen perception by NLRs in plants and animals: Parallel worlds. Bioessays **38**:769.

Figueroa, M., Ortiz, D., and Henningsen, E.C. (2021). Tactics of host manipulation by intracellular effectors from plant pathogenic fungi. Curr. Opin. Plant Biol. **62**, 102054.

Förderer, A., Li, E., Lawson, A.W., Deng, Y.N., Sun, Y., Logemann, E., Zhang, X., Wen, J., Han, Z., Chang, J., et al. (2022). A wheat resistosome defines common principles of immune receptor channels. Nature **610**:532–539.

Frantzeskakis, L., Kracher, B., Kusch, S., Yoshikawa-Maekawa, M., Bauer, S., Pedersen, C., Spanu, P.D., Maekawa, T., Schulze-Lefert, P., and Panstruga, R. (2018). Signatures of host specialization and a recent transposable element burst in the dynamic one-speed genome of the fungal barley powdery mildew pathogen. BMC Genom. **19**:381.

Gehl, C., Kaufholdt, D., Hamisch, D., Bikker, R., Kudla, J., Mendel, R.R., and Hänsch, R. (2011). Quantitative analysis of dynamic protein-protein interactions in planta by a floated-leaf luciferase complementation imaging (FLuCI) assay using binary Gateway vectors. Plant J. **67**:542–553.

Giménez, M.J., Pistón, F., and Atienza, S.G. (2011). Identification of suitable reference genes for normalization of qPCR data in comparative transcriptomics analyses in the Triticeae. Planta **233**:163–173.

Gourcilleau, D., Lenne, C., Armenise, C., Moulia, B., Julien, J.-L., Bronner, G., and Leblanc-Fournier, N. (2011). Phylogenetic Study of Plant Q-type C2H2 Zinc Finger Proteins and Expression Analysis

of Poplar Genes in Response to Osmotic, Cold and Mechanical Stresses. DNA Res. **18**:77–92.

Harvey, S., Kumari, P., Lapin, D., Griebel, T., Hickman, R., Guo, W., Zhang, R., Parker, J.E., Beynon, J., Denby, K., and Steinbrenner, J. (2020). Downy Mildew effector HaRxL21 interacts with the transcriptional repressor TOPLESS to promote pathogen susceptibility. PLoS Pathog. **16**, e1008835.

He, Q., McLellan, H., Boevink, P.C., and Birch, P.R.J. (2020). All Roads Lead to Susceptibility: The Many Modes of Action of Fungal and Oomycete Intracellular Effectors. Plant Commun. **1**, 100050.

Hewitt, T., Müller, M.C., Molnár, I., Mascher, M., Holušová, K., Šimková, H., Kunz, L., Zhang, J., Li, J., Bhatt, D., et al. (2021). A highly differentiated region of wheat chromosome 7AL encodes a Pm1a immune receptor that recognizes its corresponding AvrPm1a effector from Blumeria graminis. New Phytol. **229**:2812–2826.

Himmelbach, A., Zierold, U., Hensel, G., Riechen, J., Douchkov, D., Schweizer, P., and Kumlehn, J. (2007). A set of modular binary vectors for transformation of cereals. Plant Physiol. **145**:1192–1200.

Hong, Z., Shikai, L., Changyou, W., and Wanquan, J. (2018). The role of transcription factor in wheat defense against pathogen and its prospect in breeding. J. Plant Biol. Crop Res. **1**.

Huang, J., Sun, S., Xu, D., Lan, H., Sun, H., Wang, Z., Bao, Y., Wang, J., Tang, H., and Zhang, H. (2012). A TFIIIA-type zinc finger protein confers multiple abiotic stress tolerances in transgenic rice (Oryza sativa L.). Plant Mol. Biol. **80**:337–350.

Hurni, S., Brunner, S., Buchmann, G., Herren, G., Jordan, T., Krukowski, P., Wicker, T., Yahiaoui, N., Mago, R., and Keller, B. (2013). Rye Pm8 and wheat Pm3 are orthologous genes and show evolutionary conservation of resistance function against powdery mildew. Plant J. **76**:957–969.

Hurni, S., Scheuermann, D., Krattinger, S.G., Kessel, B., Wicker, T., Herren, G., Fitze, M.N., Breen, J., Presterl, T., Ouzunova, M., and Keller, B. (2015). The maize disease resistance gene Htn1 against northern corn leaf blight encodes a wall-associated receptor-like kinase. Proc. Natl. Acad. Sci. USA **112**:8780–8785.

IWGSC. (2018). Shifting the limits in wheat research and breeding using a fully annotated reference genome. Science **80**:361.

Jay, F., Brioudes, F., and Voinnet, O. (2023). A contemporary reassessment of the enhanced transient expression system based on the tombusviral silencing suppressor protein P19. Plant J. **113**:186–204.

Jin, Y., Liu, H., Gu, T., Xing, L., Han, G., Ma, P., Li, X., Zhou, Y., Fan, J., Li, L., et al. (2022). Pm2b, a CC-NBS-LRR protein, interacts with TaWRKY76-D to regulate powdery mildew resistance in common wheat. Front. Plant Sci. **13**:973065.

Kagale, S., and Rozwadowski, K. (2011). EAR motif-mediated transcriptional repression in plants: An underlying mechanism for epigenetic regulation of gene expression. Epigenetics **6**:141–146.

Kubo, K. i, Sakamoto, A., Kobayashi, A., Rybka, Z., Kanno, Y., Nakagawa, H., and Takatsuji, H. (1998). Cys2/His2 zinc-finger protein family of petunia: evolution and general mechanism of target-sequence recognition. Nucleic Acids Res. **26**:608–615.

Kunz, L., Sotiropoulos, A.G., Graf, J., Razavi, M., Keller, B., and Müller, M.C. (2023). The broad use of the Pm8 resistance gene in wheat resulted in hypermutation of the AvrPm8 gene in the powdery mildew pathogen. BMC Biol. **21**. 29-15.

Lindner, S., Keller, B., Singh, S.P., Hasenkamp, Z., Jung, E., Müller, M.C., Bourras, S., and Keller, B. (2020). Single residues in the LRR domain of the wheat PM3A immune receptor can control the strength and the spectrum of the immune response. Plant J. **104**:200–214.

Lo Presti, L., Lanver, D., Schweizer, G., Tanaka, S., Liang, L., Tollot, M., Zuccaro, A., Reissmann, S., and Kahmann, R. (2015). Fungal Effectors and Plant Susceptibility. Annu. Rev. Plant Biol. **66**:513–545.

Lu, X., Kracher, B., Saur, I.M.L., Bauer, S., Ellwood, S.R., Wise, R., Yaeno, T., Maekawa, T., and Schulze-Lefert, P. (2016). Allelic barley MLA immune receptors recognize sequence-unrelated avirulence effectors of the powdery mildew pathogen. Proc. Natl. Acad. Sci. USA **113**:E6486–E6495.

Manser, B., Koller, T., Praz, C.R., Roulin, A.C., Zbinden, H., Arora, S., Steuernagel, B., Wulff, B.B.H., Keller, B., and Sánchez-Martín, J. (2021). Identification of specificity-defining amino acids of the wheat immune receptor Pm2 and powdery mildew effector AvrPm2. Plant J. **106**:993–1007.

Müller, M.C., Praz, C.R., Sotiropoulos, A.G., Menardo, F., Kunz, L., Schudel, S., Oberhänsli, S., Poretti, M., Wehrli, A., Bourras, S., et al. (2019). A chromosome-scale genome assembly reveals a highly dynamic effector repertoire of wheat powdery mildew. New Phytol. **221**:2176–2189.

Müller, M.C., Kunz, L., Schudel, S., Lawson, A.W., Kammerecker, S., Isaksson, J., Wyler, M., Graf, J., Sotiropoulos, A.G., Praz, C.R., et al. (2022). Ancient variation of the AvrPm17 gene in powdery mildew limits the effectiveness of the introgressed rye Pm17 resistance gene in wheat. Proc. Natl. Acad. Sci. USA **119**:1–12.

Nakagawa, T., Suzuki, T., Murata, S., Nakamura, S., Hino, T., Maeo, K., Tabata, R., Kawai, T., Tanaka, K., Niwa, Y., et al. (2007). Improved gateway binary vectors: High-performance vectors for creation of fusion constructs in transgenic analysis of plants. Biosci. Biotechnol. Biochem. **71**:2095–2100.

Ngou, B.P.M., Ahn, H.-K., Ding, P., and Jones, J.D.G. (2021). Mutual potentiation of plant immunity by cell-surface and intracellular receptors. Nat **592**:110–115.

Nguyen, Q.M., Iswanto, A.B.B., Son, G.H., and Kim, S.H. (2021). Recent advances in effector-triggered immunity in plants: New pieces in the puzzle create a different paradigm. Int. J. Mol. Sci. **22**, 4709.

Ogata, T., Kida, Y., Arai, T., Kishi, Y., Manago, Y., Murai, M., and Matsushita, Y. (2012). Overexpression of tobacco ethylene response factor NtERF3 gene and its homologues from tobacco and rice induces hypersensitive response-like cell death in tobacco. J. Gen. Plant Pathol. **78**:8–17.

Ohta, M., Matsui, K., Hiratsu, K., Shinshi, H., and Ohme-Takagi, M. (2001). Repression Domains of Class II ERF Transcriptional Repressors Share an Essential Motif for Active Repression. Plant Cell **13**:1959–1968.

Parlange, F., Roffler, S., Menardo, F., Ben-David, R., Bourras, S., McNally, K.E., Oberhaensli, S., Stirnweis, D., Buchmann, G., Wicker, T., and Keller, B. (2015). Genetic and molecular characterization of a locus involved in avirulence of Blumeria graminis f. sp. tritici on wheat Pm3 resistance alleles. Fungal Genet. Biol. **82**:181–192.

Pennington, H.G., Jones, R., Kwon, S., Bonciani, G., Thieron, H., Chandler, T., Luong, P., Morgan, S.N., Przydacz, M., Bozkurt, T., et al. (2019). The fungal ribonuclease-like effector protein CSEP0064/BEC1054 represses plant immunity and interferes with degradation of host ribosomal RNA. PLoS Pathog. **15**, e1007620.

Petre, B., and Kamoun, S. (2014). How Do Filamentous Pathogens Deliver Effector Proteins into Plant Cells? PLoS Biol. **12**, e1001801.

Praz, C.R., Bourras, S., Zeng, F., Sánchez-Martín, J., Menardo, F., Xue, M., Yang, L., Roffler, S., Böni, R., Herren, G., et al. (2017). AvrPm2 encodes an RNase-like avirulence effector which is conserved in the two different specialized forms of wheat and rye powdery mildew fungus. New Phytol. **213**:1301–1314.

Praz, C.R., Menardo, F., Robinson, M.D., Müller, M.C., Wicker, T., Bourras, S., and Keller, B. (2018). Non-parent of origin expression of numerous effector genes indicates a role of gene regulation in host adaption of the hybrid triticale powdery mildew pathogen. Front. Plant Sci. **9**:49.

Ridout, C.J., Skamnioti, P., Porritt, O., Sacristan, S., Jones, J.D.G., and Brown, J.K.M. (2006). Multiple Avirulence Paralogues in Cereal Powdery Mildew Fungi May Contribute to Parasite Fitness and Defeat of Plant Resistance. Plant Cell **18**:2402–2414.

Robin, G.P., Kleemann, J., Neumann, U., Cabre, L., Dallery, J.-F., Lapalu, N., and O'Connell, R.J. (2018). Subcellular Localization Screening of Colletotrichum higginsianum Effector Candidates Identifies Fungal Proteins Targeted to Plant Peroxisomes, Golgi Bodies, and Microtubules. Front. Plant Sci. **9**:562.

Sánchez-Martín, J., Steuernagel, B., Ghosh, S., Herren, G., Hurni, S., Adamski, N., Vrána, J., Kubaláková, M., Krattinger, S.G., Wicker, T., et al. (2016). Rapid gene isolation in barley and wheat by mutant chromosome sequencing. Genome Biol. **17**:221–227.

Sánchez-Martín, J., Widrig, V., Herren, G., Wicker, T., Zbinden, H., Gronnier, J., Spörri, L., Praz, C.R., Heuberger, M., Kolodziej, M.C., et al. (2021). Wheat Pm4 resistance to powdery mildew is controlled by alternative splice variants encoding chimeric proteins. Nat. Plants **7**:327–341.

Saur, I.M., Bauer, S., Kracher, B., Lu, X., Franzeskakis, L., Müller, M.C., Sabelleck, B., Kümmel, F., Panstruga, R., Maekawa, T., and Schulze-Lefert, P. (2019). Multiple pairs of allelic MLA immune receptor-powdery mildew AVRA effectors argue for a direct recognition mechanism. Elife **8**, e44471.

Saur, I.M.L., Panstruga, R., and Schulze-Lefert, P. (2021). NOD-like receptor-mediated plant immunity: from structure to cell death. Nat. Rev. Immunol. **21**:305–318.

Scofield, S.R., Huang, L., Brandt, A.S., and Gill, B.S. (2005). Development of a virus-induced gene-silencing system for hexaploid wheat and its use in functional analysis of the Lr21-mediated leaf rust resistance pathway. Plant Physiol. **138**:2165–2173.

Shen, Q.-H., Saijo, Y., Mauch, S., Biskup, C., Bieri, S., Keller, B., Seki, H., Ulker, B., Somssich, I.E., and Schulze-Lefert, P. (2007). Nuclear activity of MLA immune receptors links isolate-specific and basal disease-resistance responses. Science **315**:1098–1103.

Toruño, T.Y., Stergiopoulos, I., and Coaker, G. (2016). Plant-Pathogen Effectors: Cellular Probes Interfering with Plant Defenses in Spatial and Temporal Manners. Annu. Rev. Phytopathol. **54**:419–441.

Troch, V., Audenaert, K., Vanheule, A., Bekaert, B., Höfte, M., and Haesaert, G. (2014). The importance of non-penetrated papillae formation in the resistance response of triticale to powdery mildew (Blumeria graminis). Plant Pathol. **63**:129–139.

Wang, J., Wang, J., Hu, M., Wu, S., Qi, J., Wang, G., Han, Z., Qi, Y., Gao, N., Wang, H.-W., et al. (2019). Ligand-triggered allosteric ADP release primes a plant NLR complex. Science (80- **364**. eaav5868–20.

Wicker, T., Oberhaensli, S., Parlange, F., Buchmann, J.P., Shatalina, M., Roffler, S., Ben-David, R., Doležel, J., Šimková, H., Schulze-Lefert, P., et al. (2013). The wheat powdery mildew genome shows the unique evolution of an obligate biotroph. Nat. Genet. **45**:1092–1096.

Wu, R., and Citovsky, V. (2017). Adaptor proteins GIR1 and GIR2. II. Interaction with the co-repressor TOPLESS and promotion of histone deacetylation of target chromatin. Biochem. Biophys. Res. Commun. **488**:609–613.

Yang, J., Liu, Y., Yan, H., Tian, T., You, Q., Zhang, L., Xu, W., and Su, Z. (2018). PlantEAR: Functional Analysis Platform for Plant EAR Motif-Containing Proteins. Front. Genet. **9**:590.

Yuan, M., Jiang, Z., Bi, G., Nomura, K., Liu, M., Wang, Y., Cai, B., Zhou, J.M., He, S.Y., and Xin, X.F. (2021). Pattern-recognition receptors are required for NLR-mediated plant immunity. Nature **592**:105–109.

Zhang, D., Gao, Z., Zhang, H., Yang, Y., Yang, X., Zhao, X., Guo, H., Nagalakshmi, U., Li, D., Dinesh-Kumar, S.P., and Zhang, Y. (2023). The MAPK-Alfin-like 7 module negatively regulates ROS scavenging genes to promote NLR-mediated immunity. Proc. Natl. Acad. Sci. USA **120**, e2214750120.

Zhou, J.M., and Zhang, Y. (2020). Plant Immunity: Danger Perception and Signaling. Cell **181**:978–989.